Petroleum Science 21 (2024) 3587–3611

Contents lists available at ScienceDirect

Petroleum Science

journal homepage: www.keaipublishing.com/en/journals/petroleum-science

Original Paper

Model-based interpretation of bottomhole pressure records during matrix treatments in layered formations

Igor Reznikov [a, *], Dmitry Abdrazakov [b], Dimitry Chuprakov [b]

[a] Schlumberger Moscow Research, Leningradskoe shosse, bldg. 16A, corp.3, Moscow, 125171, Russian Federation
[b] Novosibirsk Technology Center, 1/10 Zelenaya Gorka str, Novosibirsk, 630060, Russian Federation

ARTICLE INFO

Article history:
Received 10 May 2023
Received in revised form
18 March 2024
Accepted 30 May 2024
Available online 1 June 2024

Edited by Jie Hao

Keywords:
Matrix treatment
Inverse problem
Forward problem
Skin factor
Interpretation

ABSTRACT

During injection treatments, bottomhole pressure measurements may significantly mismatch modeling results. We devise a computationally effective technique for interpretation of fluid injection in a wellbore interval with multiple geological layers based on the bottomhole pressure measurements. The permeability, porosity and compressibility in each layer are initially setup, while the skin factor and partitioning of injected fluids among the zones during the injection are found as a solution of the problem. The problem takes into account Darcy flow and chemical interactions between the injected acids, diverter fluids and reservoir rock typical in modern matrix acidizing treatments. Using the synchronously recorded injection rate and bottomhole pressure, we evaluate skin factor changes in each layer and actual fluid placement into the reservoir during different pumping jobs: matrix acidizing, water control, sand control, scale squeezes and water flooding. The model is validated by comparison with a simulator used in industry. It gives opportunity to estimate efficiency of a matrix treatment job, role of every injection stage, and control fluid delivery to each layer in real time. The presented interpretation technique significantly improves accuracy of matrix treatments analysis by coupling the hydrodynamic model with records of pressure and injection rate during the treatment.

1. Introduction

Well testing models based on the transient pressure analysis approach are important tools for obtaining information about the reservoir and fluid filtration (Matthews and Russell, 1967). These approaches apply to fluid flow in the presence of a hydraulic fracture (Cinco-Ley and Samaniego, 1981) or natural fractures (Biryukov and Kuchuk, 2012; Kuchuk et al., 2015). In acidizing applications, this method is also widely used for both fracture and matrix acidizing (McLeod and Coulter, 1969). Matrix acidizing is a stimulation process in which fluid (typically acid) is injected into the wellbore at a pressure below the breakdown pressure and then filtrates into the reservoir rock. The primary goal of matrix treatment is to reduce the near-wellbore zone damage and thereby increase the permeability of the rock. The job is considered successful if both technical and economic objectives are achieved. One defining physical parameter is skin factor, which should decrease in the near-wellbore zone after successful treatment. To estimate the effectiveness of a stimulation job performed, it is necessary to create real-time monitoring models.

The first monitoring methods based on pressure transient analysis and steady-state Darcy flow were presented by McLeod and Coulter (1969) and Paccaloni et al. (1979, 1988) respectively. Both of these approaches monitored changes in skin factors during the treatment, but accuracy was not high. Later, Prouvost and Economides (1987, 1989) presented a more accurate method based on the transient solution, which is much more suitable for the treatment problem. This solution was later improved by other authors (Chan et al., 2003; Hill and Zhu, 1996; Montgomery et al., 1995). In this paper, we will also rely on this approach as the most correct one for the multi-zone structure, as well as advanced diverter technologies.

In addition to the hydrodynamic aspects of fluid filtration into the formation, matrix treatment is also based on chemical interactions of the fluid with the rock. Lund et al. (1973, 1975) studied the most common reactions of hydrochloric acid with dolomite ($CaMg(CO_3)_2$) and limestone ($CaCO_3$). The injected acid corrodes

* Corresponding author.
E-mail address: ireznikov@slb.com (I. Reznikov).

https://doi.org/10.1016/j.petsci.2024.05.027

Nomenclature

Roman letter

B	Constant of analytical solution introduced in Eq. (6)
c_t	Total zone compressibility
C	Concentration
D	Diffusion coefficient
E_f^0	Reaction rate constant
h	Zone thickness
k	Zone permeability
L_{wh}	Wormhole length
$\mathscr{L}$	Radial depth of fluid filtration into zone
MW	Molecular weight
N_{Da}	Damköhler number
N_{Pe}	Peclet number
p	Pressure
p_u	Unit-rate pressure introduced in Eq. (7)
p_{wf}	Bottomhole pressure
P_{sc}	Pressure scale introduced in Eq. (6)
Q	Total injection rate to the well
q	Zone flow rate
R_w	Wellbore radius
R'_w	Effective wellbore radius
$\mathscr{R}$	Gas constant
r	Radius
r_{At}	Rate of acid consumption at the tip
S	Skin factor
$\widehat{S}$	Uniform skin multiplier
T_D	Dimensionless time
T'_D	Effective dimensionless time
$\mathscr{T}$	Reaction temperature
$\mathscr{T}_0^L$	Temperature corrections for hydrochloric acid-limestone reaction
$\mathscr{T}_0^D$	Temperature corrections for hydrochloric acid-dolomite reaction
t	Time
U_S	Normalized skin velocity
V	Zone injected volume

Greek letter

α	Order of chemical reaction introduced in Eq. (12)
β	Power introduced in Eq. (23)
γ	Power introduced in Eq. (23)
ΔE	Activation energy
λ_{BT}	Structure efficiency parameter
μ	Viscosity of the injected fluid
ν	Ratio of stoichiometric coefficients
ρ	Density of the fluid or material
χ_t	Volumetric dissolving power at the tip

Mathematical function

F_n	Function defined in Section 3.3
K_0	Modified Bessel function of the second kind of zero order
K_1	Modified Bessel function of the second kind of first order

Subscripts and superscripts

1z	One zone
A	Acid
D	Dimensionless
Dolo	Dolomite
Lime	Limestone
M	Mineral
m	Index for zone number
n	Index for time moment
t	Tip

Acronyms

$CaCl_2$	Calcium chloride
$CaCO_3$	Calcium carbonate (limestone)
$CaMg(CO_3)_2$	Calcium magnesium carbonate (dolomite)
CO_2	Carbon dioxide
CRF	Cumulative redistributed fluid volume
DHG	Downhole gauge
HCl	Hydrochloric acid
H_2O	Dihydrogen oxide
MaTI	Matrix treatment interpreter
$MgCl_2$	Magnesium chloride
MSE	Mean square error
OPS	Open path sequence
PLT	Production logging tool
RF	Redistributed fluid volume
RS	Reference solution
SPRA	Single-phase retarded acid
VES	Viscoelastic surfactant-based

the rock walls, resulting in the formation of wormholes, which are highly conductive channels that effectively increase the permeability of the rock. There are many mathematical models that describe wormhole growth (Buijse, 2000; Buijse et al., 2005; Daccord et al., 1993; Daccord and Lenormand, 1987; Fredd and Fogler, 1998; Furui et al., 2011; Gdanski, 1999; Hoefner and Fogler, 1988; Huang et al., 1999, 2000; Wang et al., 1993).

In this paper, we will use the approach presented by Fredd and Fogler (1998, 1999) to relate wormhole growth to the skin factor. These authors have shown that wormhole formation is governed by the Damköhler number (N_{Da}). They discovered that for all reactions there is an optimal Damköhler number of about 0.29, which describes the minimum number of pore volumes required to form a dominant wormhole. These results have also been used as the basis for industrial simulators. Panga et al. (2002, 2004) described reactive dissolution in porous media as a coupling between processes occurring at the Darcy scale and at the pore scale. This model is based on acid flow and transport equations and pays special attention to the determination of the acid filtration model: mass transfer controlled or kinetically controlled. The description of optimal injection rate and dissolution patterns is based on several dimensionless constants: Damköhler number, Thiele modulus, and acid capacity number.

The process of acid-rock interaction is well studied. There are many models that, with varying degrees of accuracy and under different assumptions, can estimate the length of emanating wormholes and thus predict the final skin factor obtained after acidizing. However, the achievement of the desired result of a treatment job with reservoir rock heterogeneity is a challenge. For example, the presence of the so-called “thief zone” (a layer of limited thickness with high permeability) can strongly influence the spatial distribution of acids, because a lion’s share of the total

fluid will flow into this zone and create dominant wormholes, while less permeable neighboring zones remain untreated (Pye et al., 1970). To avoid this problem and control the fluid distribution process, matrix treatment jobs require special fluid diversion techniques. In the industry, fluid diversion methods are classified as mechanical and chemical, the former referring to solid particles that physically plug the fluid path and the latter referring to high viscosity fluids. For research purposes, it is more convenient to classify diversion methods according to the components of Darcy's law that each method addresses (Abdrazakov et al., 2019):

- Methods that reduce the height available for flow ("h"): dividing the interval by packers,
- Methods that increase the skin factor of the surface area exposed to the flow ("s"): pumped-in particles,
- Methods that increase the viscosity of the filtrating fluid ("μ"): viscous fluids and foams.

In general, there are many researchers who have studied the influence of diverting agents and self-diverting acids on the flow of acids into a permeable rock (Crowe, 1971; Doerler and Prouvost, 1987; Prouvost and Economides, 1989; Tardy et al., 2007; Cohen et al., 2010). Many of these approaches rely on experimental data and cannot be used in the general case.

Carbonate formations contain around 50% of recoverable oil and gas reserves (Al-Shargabi et al., 2023). There are multiple studies based on the carbonate acidizing modelling. Majority of carbonate formations are strongly heterogeneous. They are often considered as a layered formation with different mechanical properties, such as permeability, porosity, lithology, and reservoir pressure. The successful design and analysis of matrix acidizing treatments in the layered formations depends on the following two major components:

1. The acid-rock interaction modeling at different scales. This component has been receiving significant attention in research due to ability to validate theories by means of precise laboratory tests (Akanni and Nasr-El-Din, 2015; Ali and Nasr-El-Din, 2018; Jia et al., 2021; Schwalbert et al., 2017; Turegeldieva et al., 2016; Yuan and Qin, 2020).
2. Understanding of the injected fluid distribution between heterogeneous reservoir layers. Usually, this understanding gets complicated by large uncertainty of reservoir properties and mismatch between the log-derived properties and actual properties of layers, when the injection is performed.

The largest error during analysis of matrix acidizing treatments comes from the second component, i.e., incorrect assumptions of reservoir properties and injectivity profile, rather than from acid-rock interaction models. There are several papers that discuss possible stimulation scenarios for multilayered rock structures (Al-Tamimi and El-Mzien, 1987; Núñez et al., 2009; Panjalizadeh et al., 2021; Pongratz et al., 2005; Ramondenc et al., 2013). However, only few of them present any reliable mathematical model.

From the review above, it becomes clear that matrix treatment is a complex process that includes:

1. Fluid injection into the wellbore, which is then filtered in multiple zones of reservoir rock near the wellbore with different filtration and lithological properties;
2. Chemical interactions of acids with the rock resulting in wormhole initiation and growth;
3. Redirection of flow between zones when the diverter is injected.

Transient pressure models can monitor the evolution of the skin factor during the injection job. Wormhole models can describe the interactions of acid with rock. To the best of our knowledge, there is no model that combines both the physical and chemical components of matrix treatment and can simultaneously describe this process for the multi-zone structure of the formation. In addition, it is still necessary to develop a model that can predict fluid distribution between zones and estimate the skin factor in each zone in real time using field data such as pressure and total flowrate profiles. Our study is bridging this gap by improving analysis of the dynamic fluid distribution during matrix treatments in real time. Therefore, our goal here is to create a simulator that would run fast enough for any type of well injection treatment, including acidizing. To achieve this goal, we simplify the physics of acid-rock interactions to a certain extent, which we believe is not the major source of analysis inaccuracy in the field today. As a result, in this work, we obtain the model that (i) is expected to represent the fluid distribution during matrix acidizing treatments more realistically compared to the models built only on logs and lacking the actual treating pressure as an input, and (ii) fast enough to be applied for the real-time fluid distribution analysis.

The approach we develop in this paper is referred to as the inverse problem. Both the total injection rate and bottomhole pressure are taken as an input, and rock properties (e.g., skin factor) are determined as a solution. Hence, even if the filtration problem remains linear, we now deal with solving non-linear equations. A reliable and computationally efficient method is required to accurately determine the root. Typical problems which arise during the root-searching process include poor convergence, possible multiple roots, and existence of stationary points. The Newton-Raphson method and its modification, the Muller method (Muller, 1956), are considered the most robust for solving non-linear equations. Their root-searching process is iterative, fast, and simple, but the success heavily depends on the initial root approximation. On the contrary, it is also possible to use hybrid methods (Brent, 1971; Chandrupatla, 1997; Ridders, 1979), which are independent of the initial approximation, but use the bracketing technique. In the context of our problem, it is necessary to determine both the initial approximation and brackets near the root with sufficient reliability. Testing effectiveness of various methods in solving the inverse filtration problem is another important goal of this work.

The paper has the following structure. In the second section, we build a mathematical model of fluid filtration in a multilayered formation. The model couples fluid filtration with the growth of wormholes in zones caused by the reaction of injected acids with rock. In the context of the model description, we describe the procedure of inverse problem solution, which allows to calculate time changes of rock properties, skin factor and flow rates in all zones. In the third section, we describe the development of numerical simulator and evaluate its sensitivity to various parameters and computational speed for several field cases. In the fourth section, we present the verification results that were obtained after comparing the simulator with some analytical solutions and an industrial solver. The fifth section presents the full cycle of interpretation of field cases. It includes description of the input data, their preprocessing and output results. This section also shows a comparison of the results with production logging tool (PLT) data and estimates economic efficiency of the treatment carried out. The paper wraps up with the discussion of possible improvements of the model in future, and list of main conclusions. Important mathematical derivations used in the verification section are presented in detail in Appendices A and B.

2. The model

2.1. Problem statement

We consider a matrix treatment job fulfilled in an isolated section of a wellbore. The treated wellbore segment is contacted by M horizontal rock layers (zones) with different hydro-mechanical properties. During fluid injection into a wellbore, the injected fluid penetrates all crossed layers with different velocity and volumetric rates q_n and results in building different skin factors S_n (Fig. 1(a) and (b)). The skin factor and flow rate both change over the injection time in each zone, as (Fig. 1, (c)) indicates.

The zones are typically specified by their top and bottom boundaries, and hence, their thickness $h^{(m)}$, and estimated permeability $k^{(m)}$ ($m = \overline{1,M}$). Hereafter, m is the index of a reservoir zone. These estimates may be far inaccurate but serve as initial guess of zone property characterization. Other properties required by models are porosity $\varphi^{(m)}$ and compressibility $c^{(m)}$ are often either reported or calculated using engineering correlations. The viscosity of injected fluids μ is another important factor, that heavily influences the calculations. The injection rate and downhole pressure transients during treatment jobs are often properly recorded with sufficiently fine timestep (typically, 1 s). Both injection rate and pressure can vary but must stay positive during the whole treatment job. If by any chance, the recorded values change the sign or show zero values, they must be excluded from the interpretation problem, as occurred due to irrelevant effects, e.g., wellbore section isolation losses, or other failures during the job or measurements.

The total injected fluid volume can be unequally distributed among all zones contacting the treating wellbore section (Fig. 1(a) and (b)). The wellbore pressure is uniform across all zones. Solution of the filtration problem gives the volumetric distribution of flow rates $q^{(m)}(t)$ and injected fluid volumes $V^{(m)}(t)$ during and at the end of the job, so that

$$\begin{aligned} p_{wf}(t_i) &= p^{(m)}(t_i) \\ Q(t_i) &= \sum_{m=1}^{M} q^{(m)}(t_i) \\ V(t) = \int_0^t Q(t')\mathrm{d}t' &= \sum_{m=1}^{M} V^{(m)}(t) \end{aligned} \tag{1}$$

It is important to underline that here and after flow rates and volumes are specific values and are normalized on the zonal width. The physical dimensions of flow rates and injected fluid volumes are $\frac{m^2}{s}$ and m^2 respectively. The injection treatment is also related to changes of hydro-mechanical properties of treated rock layers, for instance, increase of permeability of near wellbore rock because of acidizing, or plugging because of diverter fluid injection. The solution of inverse problem must evaluate the transient change of zone properties during the treatment, which complies with known variations of total injection rate and wellbore pressure. The change of permeable properties near wellbore can be accounted for by means of the skin factor. The solution must couple the injection rate, wellbore pressure, transient changes of zone properties during the treatment, and a picture of total injected volume partitioning between zones. For constructing the model, we assume that

- The injected fluids are low compressible
- The wellbore walls are stiff, so all fluids injected to a wellbore immediately penetrate the formation
- Two-dimensional radial flow within each zone

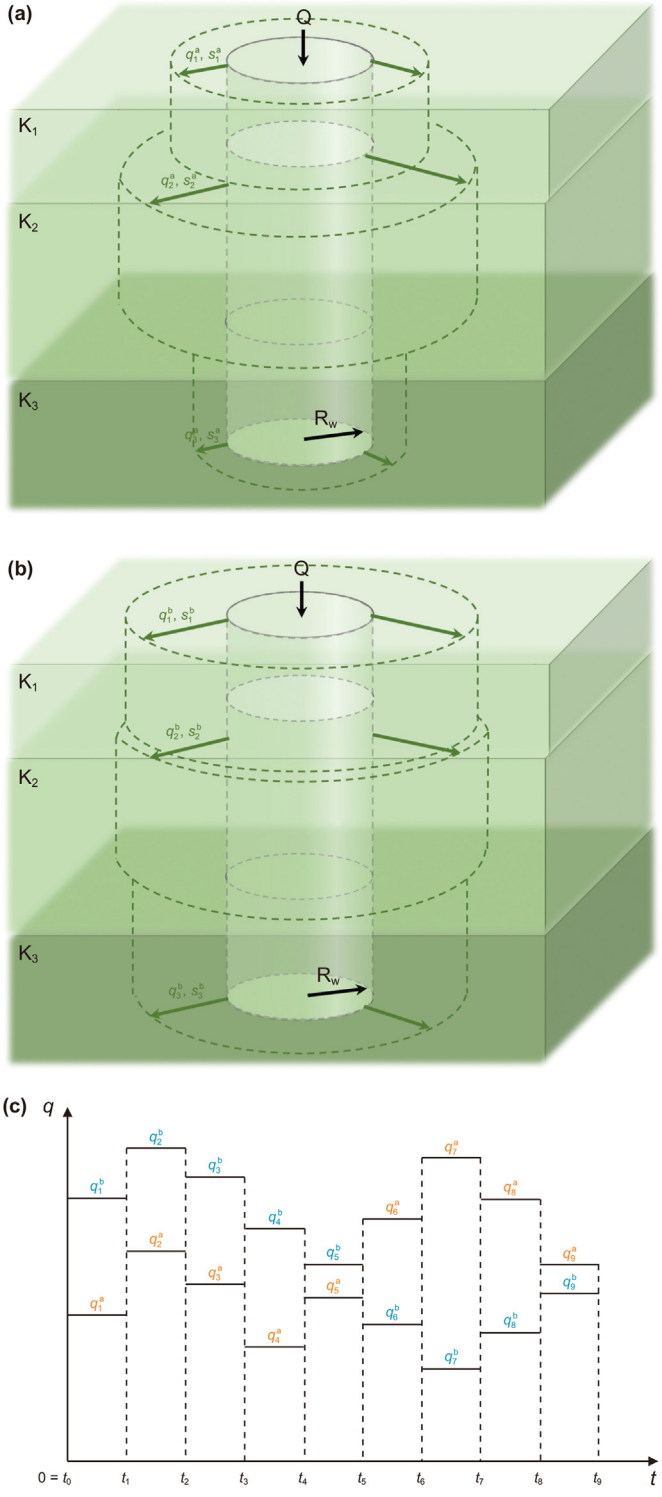

Fig. 1. Filtration of fluid from the wellbore into the multizonal heterogeneous reservoir (with zone permeabilities $K_2 \gg K_1 > K_3$, and zone skin factors denoted by s) for two arbitrary injection scenarios **(a)** and **(b)**. Injection scenario is characterized by injection rate, injected fluid type, and volume. Fluid is pumped at total rate Q, and this total rate is distributed into zonal volumetric rates q_1, q_2, q_3 differently for different injection scenarios. **(c)** Zonal rates change in time for two different injection scenarios. Orange font describes the evolution of the fluid flow rate in time for the injection scenario (a); blue font describes the evolution of the fluid flow rate in time for the injection scenario (b).

- Piston-like displacement of reservoir fluid by injected fluids within each zone

Given these assumptions, filtration of injected fluids from a wellbore to the m-th zone can be described by the following linear pressure diffusion equation (Barenblatt et al., 1972):

$$\frac{\partial p^{(m)}}{\partial t} = \frac{D^{(m)}}{r}\frac{\partial p^{(m)}}{\partial r}\left(r\frac{\partial p^{(m)}}{\partial r}\right) \tag{2}$$

where $D^{(m)}$ is the diffusion coefficient of m-th zone, $p^{(m)}$ is the fluid pressure in the m-th zone.

$$D^{(m)} = \frac{k^{(m)}}{\varphi^{(m)} c_{\mathrm{t}}^{(m)} \mu} \tag{3}$$

where $k^{(m)}$ is the zone permeability, $\varphi^{(m)}$ is the zone porosity, $c_{\mathrm{t}}^{(m)}$ is the total zone compressibility, and μ is the injected fluid viscosity. Eq. (2) is supplemented by two boundary conditions. The first one is the prescribed flow at the inlet of the well:

$$\left.\frac{\partial p^{(m)}}{\partial r}\right|_{r=R_{\mathrm{w}}} = -\frac{q^{(m)}\mu}{2\pi k^{(m)} R_{\mathrm{w}} h^{(m)}} \tag{4}$$

Here $q^{(m)}$ is the fluid injection rate to m-th zone, R_{w} is the wellbore radius, $h^{(m)}$ is the zone height. We suppose that for acidizing problems reservoir boundaries do not affect the process. At the infinite distance from a wellbore, we get the second boundary condition:

$$\left.p^{(m)}\right|_{r\to\infty} = 0 \tag{5}$$

2.2. The solution of multilayer filtration problem

The solution of a radial filtration problem is well known (Matthews and Russell, 1967). It is often expressed in terms of the logarithmic law of pressure change in a wellbore at a constant injection rate. For matrix treatment, however, this solution is not always applicable, since the dimensionless time in low permeable zones can be small. The widely used logarithmic approximation does not hold in them. To account for both early and large time asymptotes of this solution, we introduce the following more accurate analytical approximation of a bottomhole pressure for constant injection rate conditions (see Appendix A: Improved approximation for transient radial flow for derivation).

$$p_{\mathrm{wf}}\left(T_{\mathrm{D}}^{(m)}\right) = P_{\mathrm{sc}}^{(m)}\sqrt{BT_{\mathrm{D}}^{(m)}}\,\frac{K_0\left(\sqrt{1/BT_{\mathrm{D}}^{(m)}}\right)}{K_1\left(\sqrt{1/BT_{\mathrm{D}}^{(m)}}\right)} \tag{6}$$

where p_{wf} is the wellbore pressure, $P_{\mathrm{sc}}^{(m)} = q^{(m)}\mu/[2\pi k^{(m)} h^{(m)}]$ is the typical scale of wellbore pressure increment, $T_{\mathrm{D}}^{(m)} = tD^{(m)}/R_{\mathrm{w}}^2$ is the dimensionless diffusivity time and $B = 1.38$ is the approximation constant, $K_0(\bullet)$ and $K_1(\bullet)$ are the zero-order and first-order modified Bessel functions of the second kind, respectively. According to Eq. (A.8), the dimensionless time depends on the diffusion coefficient, and thus, is different in zones. To predict the skin factor accumulation in zones during the treatment, we change Eq. (6) by using the effective wellbore radius $R_{\mathrm{w}}'^{(m)} = R_{\mathrm{w}}e^{-S^{(m)}}$ and thus, $T_{\mathrm{D}}'^{(m)} = T_{\mathrm{D}}e^{2S^{(m)}}$, and have

$$\begin{aligned} p_{\mathrm{wf}}\left(T_{\mathrm{D}}^{(m)}, S^{(m)}\right) &= P_{\mathrm{sc}}^{(m)}\sqrt{BT_{\mathrm{D}}^{(m)}}\,\frac{K_0\left(\mathrm{e}^{-S^{(m)}}\Big/\sqrt{BT_{\mathrm{D}}^{(m)}}\right)}{K_1\left(\mathrm{e}^{-S^{(m)}}\Big/\sqrt{BT_{\mathrm{D}}^{(m)}}\right)} \\ &= q^{(m)} p_{\mathrm{u}}^{(m)}\left(T_{\mathrm{D}}^{(m)}, S^{(m)}\right) \end{aligned} \tag{7}$$

where we omitted dash in the dimensionless time, $p_{\mathrm{u}}^{(m)}$ is the unit rate pressure function, $q^{(m)}$ is the fluid flow rate to the m-th zone, $S^{(m)}$ is the skin factor in the m-th zone. Eq. (7) is valid only if both pressure, injection rate and skin factor are constant. During the matrix treatment job, these parameters may substantially change, so we apply the superposition principle to Eq. (7) (Matthews and Russell, 1967):

$$\begin{aligned} p_{\mathrm{wf}}\left(T_{\mathrm{D}_n}^{(m)}, S_n^{(m)}\right) &= q_n^{(m)} p_{\mathrm{u}}^{(m)}\left(T_{\mathrm{D}_n}^{(m)} - T_{\mathrm{D}_{n-1}}^{(m)}, S_n^{(m)}\right) \\ &+ \sum_{i=1}^{n-1} q_i^{(m)}\left[p_{\mathrm{u}}^{(m)}\left(T_{\mathrm{D}_n}^{(m)} - T_{\mathrm{D}_{i-1}}^{(m)}, S_n^{(m)}\right) - p_{\mathrm{u}}^{(m)}\left(T_{\mathrm{D}_n}^{(m)} - T_{\mathrm{D}_i}^{(m)}, S_n^{(m)}\right)\right] \end{aligned} \tag{8}$$

where subscript n denotes n-th time step. The first term in the right-hand side of Eq. (8) is the contribution of fluid injection at the last timestep, while the second term is the sum of contributions from all previous time steps. Every n-th time step, this equation must be solved for the unknown zonal flow rates $q_{\mathrm{n}}^{(m)}$ and skins $S_{\mathrm{n}}^{(m)}$ given the flow rates found at all $n-1$ previous timesteps. That means that we must solve the following coupled equations for the pressure-rate coupling in each zone and the total injection rate:

$$\begin{cases} p_{\mathrm{wf}}\left(T_{\mathrm{D}_n}^{(m)}, S_n^{(m)}\right) = q_1^{(m)} p_{\mathrm{u}}^{(m)}\left(T_{\mathrm{D}_n}^{(m)} - T_{\mathrm{D}_1}^{(m)}, S_n^{(m)}\right) \\ \quad + \sum_{i=2}^{n}\left[q_i^{(m)} p_{\mathrm{u}}^{(m)}\left(T_{\mathrm{D}_n}^{(m)} - T_{\mathrm{D}_i}^{(m)}, S_n^{(m)}\right) - q_{i-1}^{(m)} p_{\mathrm{u}}^{(m)}\left(T_{\mathrm{D}_n}^{(m)} - T_{\mathrm{D}_{i-1}}^{(m)}, S_n^{(m)}\right)\right] \\ Q_n = \sum_{m=1}^{M} q_n^{(m)} \end{cases} \tag{9}$$

2.3. Coupled problem solution

Eq. (9) consists of $M+1$ equations written for $2M$ unknowns. To solve it, we add the following M equations for M variable skin factors $S_n^{(m)}$ in each zone:

$$S_n^{(m)} = S_{n-1}^{(m)} + (t_n - t_{n-1})\widehat{S}_n U_{S,n}^{(m)} \tag{10}$$

where $\widehat{S}_n$ is the uniform skin multiplier, $U_{S,n}^{(m)}$ is the normalized skin velocity, which defines relationship between the skin and properties of the m-th zone. This function is different in zones and allows to calculate the exact value of the skin factor change as a function of flow rate, lithological characteristics, temperature, and acid properties. Supplementing Eq. (9) with Eq. (10), we get a total of $2M+1$ equations for $2M+1$ variables ($q^{(m)}, S^{(m)}$ and $\widehat{S}$). The final system of Eqs. (9) and (10) has a unique solution.

To finalize the solution of the problem for complex multi-zonal structure, we derive a suitable analytical model for $U_{S,n}^{(m)}$ in Eq. (10). This function needs to describe mechanical-chemical interaction

between the injected fluid and reservoir rock and may depend on various parameters, such as

- Type of injected fluid (e.g., acid, diverter)
- Lithological composition of a reservoir
- Flow rate of fluid in each zone
- Temperature of an injected fluid

To derive the model of skin change, we investigate two cases. In the first one, we examine the interaction of ordinary hydrochloric acid (HCl) of a fixed concentration of 15% and constant properties that do not depend on pressure and temperature in the reservoir. In the second case, we assume that a diverter agent is injected instead of acid for a limited amount of time during the treatment job. The reservoir formation consists of two main types of minerals: limestone and dolomite. Other minerals are considered insoluble, so they do not affect the reaction.

To derive an analytical solution for the normalized skin velocity $U_{S,n}^{(m)}$, it is important to couple the skin and length of the generated wormhole. This can be done using the model proposed by Fredd (2000). Fredd connected the rate of wormhole growth with the acid dissolution rate as

$$\frac{dL_{wh}}{dt} = r_{At}\frac{MW_A}{\rho_A}\chi_t\lambda_{BT} \tag{11}$$

where r_{At} is the rate of acid consumption at the tip, MW_A and ρ_A are the molecular weight and density of the acid respectively, χ_t is the volumetric dissolving power at the tip, and λ_{BT} is the structure efficiency parameter. The last parameter accounts for the effects of dissolution structure and equals to one for optimal acidizing job. Lund et al. have measured the rate of acid consumption for both HCl-dolomite (1973) and HCl-limestone reactions (1975) and arrived at

$$-r_{At} = E_f^0 \exp\left(-\frac{\Delta E}{\mathscr{R}\mathscr{T}}\right)C_A^{\alpha} \tag{12}$$

where α, E_f^0, ΔE, $\mathscr{R}$ are the order of reaction, reaction rate constant, activation energy, and gas constant, respectively, C_A and $\mathscr{T}$ are the acid concentration and temperature in Kelvin at the reaction surface, respectively. Eq. (12) is suitable for both HCl-dolomite and HCl-limestone reactions, for which the constants are different. For HCl-dolomite reaction, both order of reaction and reaction rate constant are temperature-dependent. These constants as well as molecular weights and densities of minerals are given in Table 1 and Eqs. (13) and (14) (Economides and Nolte, 2000).

$$A_1 = \frac{6.18 \bullet 10^{-4}\mathscr{T}}{1 - 2 \bullet 10^{-3}\mathscr{T}} \tag{13}$$

$$A_2 = \frac{9.4 \cdot 10^{11}}{1000^{\alpha}} \tag{14}$$

Even though the equations for the reaction of acid with limestone and dolomite have the same form, the fundamental difference lies in the value of α. It is a temperature-dependent function for dolomite and is equal to 0.63 for $\mathscr{T} \sim 335K \sim 62^{\circ}C$. Using Eqs. (12)–(14), Table 1 and taking $\alpha = 0.63$ in both cases, it is feasible to write

$$-r_{At}^{Lime} = 7.291 \bullet 10^7 \exp\left(-\frac{7550}{\mathscr{T} + \mathscr{T}_0^L}\right)C_A^{0.63} \tag{15}$$

$$-r_{At}^{Dolo} = 1.211 \bullet 10^{10} \exp\left(-\frac{11320}{\mathscr{T} + \mathscr{T}_0^D}\right)C_A^{0.63} \tag{16}$$

where r_{At}^{Lime} and r_{At}^{Dolo} are the rates of acid consumption after reactions with the limestone and dolomite, respectively; $\mathscr{T}_0^L$ $\mathscr{T}_0^D$ are the temperature corrections for HCl-limestone and HCl-dolomite reactions. We introduce the constants T_0^L and T_0^D to deviate the order of reactions from the value 0.63 to more correct values. So, Eqs. (15) and (16) shall be used instead of Eq. (12) to mitigate possible errors.

The volumetric dissolving power χ_t expresses the volume of rock dissolved per volume of acid reacted. For 15% HCl, it can be evaluated as (Economides and Nolte, 2000)

$$\chi_t = 0.15\nu_M\frac{MW_M\rho_A}{MW_A\rho_M} \tag{17}$$

where ν_M is the ratio of stoichiometric coefficients, MW_M and ρ_M are the molecular weight and density of the minerals, respectively. The stoichiometric coefficients describe the amount of acid required to dissolve a given amount of mineral and can be obtained from the following chemical reaction equations for acid with limestone and dolomite, respectively (Lund et al., 1973, 1975):

$$2HCl + CaCO_3 \rightarrow CaCl_2 + CO_2 + H_2O \tag{18}$$

$$4HCl + CaMg(CO_3)_2 \rightarrow CaCl_2 + MgCl_2 + 2CO_2 + 2H_2O \tag{19}$$

From these reactions, one can get that $\nu_{Lime} = 0.5$ and $\nu_{Dolo} = 0.25$. Combining Eqs. (12)–(19) and data from Table 1, we obtain the following equations for the wormhole growth rate in pure limestone and dolomite fractions:

$$\frac{dL_{wh}^{Lime}}{dt} = 2.02 \bullet 10^8 \exp\left(-\frac{7550}{\mathscr{T} + \mathscr{T}_0^L}\right)C_A^{0.63} \tag{20}$$

$$\frac{dL_{wh}^{Dolo}}{dt} = 2.42 \bullet 10^{11} \exp\left(-\frac{11320}{\mathscr{T} + \mathscr{T}_0^D}\right)C_A^{0.63} \tag{21}$$

Generally, the wormhole growth rate is found as the superposition of Eqs. (20) and (21) and written as

$$\frac{dL_{wh}}{dt} = 10^8\left[2.02C_{Lime}\exp\left(-\frac{7550}{\mathscr{T} + \mathscr{T}_0^L}\right) + 2420C_{Dolo}\exp\left(-\frac{11320}{\mathscr{T} + \mathscr{T}_0^D}\right)\right]C_A^{0.63} \tag{22}$$

where C_{Lime} and C_{Dolo} are partial concentrations of limestone and dolomite formations in the reservoir rock. Eq. (22) fully describes the rate of wormhole development when 15% HCl acid is injected into the rock. This, however, does not give a complete understanding of how the skin factor changes in zones. In this paper, we suggest that the rate of skin change in each m-th zone depends on two parameters: the local flow rate in that zone $q^{(m)}$ and the rate of

Table 1
Constants used for describing acid-rock reaction model. Sign * denotes the dimension of reaction rate constant, which is $(kg - mol\ HCl)/\left[m^2 - s\left(\frac{kg - mol\ HCl}{m^3}\right)^{\alpha}\right]$.

Mineral\Parameter	α	$E_f^{0^*}$	$\Delta E/\mathscr{R}$, K	MW_M	ρ_M, g/cm³
Limestone	0.63	7.291*10⁷	7.55*10³	100.1	2.71
Dolomite	A_1	A_2	11.32*10³	156.3	2.88

wormhole growth $dL_{wh}^{(m)}/dt$ as follows:

$$\frac{dS^{(m)}}{dt} = q^{(m)^{\gamma}} \left(\frac{dL_{wh}^{(m)}}{dt} \right)^{\beta} \tag{23}$$

Eq. (23) means that the skin development in a zone depends on two factors: how much fluid is injected and how fast the wormhole grows. The unknown constants γ and β can be found from experiments or comparison with other industrial solvers, and they are different for different injected fluids. In this paper we focus only on interaction of 15% HCl acid with limestone and dolomite rock, so we conducted $\gamma, \beta, \mathscr{T}_0^{\mathrm{L}}$ and $\mathscr{T}_0^{\mathrm{D}}$ for these reactions only. If during matrix treatment another acid or HCl with different concentration is used, these constants need to be recalculated. In Section 4.3, we compare this model with an industrial solver and find the unknown constants γ and β. To define the skin velocity $U_{S,n}^{(m)}$, we normalize Eq. (23) as

$$U_{S,n}^{(m)} = \frac{dS^{(m)} \Big/ dt}{\max\limits_{m} \left(dS^{(m)} \Big/ dt \right)} \tag{24}$$

In the zone with the biggest skin change, we setup the normalize skin velocity equal to 1. In all other zones the value will be less, but always greater than zero. Eqs. (9), (10) and (24) fully define the mathematical problem to solve. The solution of these equations gives the unknown distribution of the skin factor in each zone over the treatment, as well as zonal flow rates and volumes.

2.4. Forward and inverse problems

The forward modeling is widely used approach (Cohen et al., 2010; Parn-anurak and Engler, 2005; Tardy et al., 2007). It requires full determination of all rock properties and laws of interaction of rock with active or reactive fluids during the injection job. Typically, such models accept the injection rate as a given boundary condition and solve for the wellbore pressure changes. At the stage of treatment job interpretation, the computed wellbore pressure must be additionally history matched to the recorded pressure to make sure that the model correctly predicts changes of rock properties. Typically, the matching is not part of the model. Alternatively, the wellbore pressure can be specified as a boundary condition at the wellbore walls. Then, the flow rate is to be computed given rock properties at every moment of time. In this paper we fix skin multiplier for an arbitrary period and assume that pressure is not recorded. This allows us to solve forward problem and calculate pressure for prescribed skin factor.

The other approach is the inverse modeling, where both wellbore pressure and injection rate are taken as an input to the model (Paccaloni, 1979; Prouvost and Economides, 1987, 1989). The model, then, solves for the change of rock properties in time. Typically, solving an inverse problem leads to the system of equations with implicit solution, because the explicit solution cannot be written. Different numerical algorithms based on gradient descent are used to calculate approximate solution of the inverse problem. Due to many uncertainties and general complexity, this approach is not as popular in literature, as forward models. In this work, we employ the special numerical algorithm to solve an inverse problem given by Eqs. (9), (10) and (24).

3. Numerical solution

The mathematical model described above requires solving Eqs. (9) and (10) numerically. For numerical solution, we propose the algorithm shown in Fig. 2. First, we read the input data recorded after the matrix treatment job. The data include measurements of bottomhole pressure, injection rate, as well as hydrodynamical and geometrical properties of zones (e.g., permeability, porosity, compressibility, lithological composition, and height). Then, as a preprocessing stage, we filter the field data records out to exclude possible acoustic noises. The acoustic pressure signals are not part of the fluid filtration model and hence, spoil correctness of the fluid filtration interpretation. After the preprocessing, we use the filtered data to solve the inverse problem (Eq. (9) and (10)). Taking the normalized skin velocity as a function of lithology and zone height from Eq. (24), we find the unknown skin multiplier $\widehat{S}_n$ numerically. After that, we calculate the skin factor and flow rates in each zone using Eqs. (9) and (10). The volumes of fluid injected into each zone $V^{(m)}(t)$ are then calculated from Eq. (1), right. The radial depth of fluid filtration into each zone is then found using the following relation:

$$\mathscr{L}^{(m)} = \frac{V^{(m)}}{\varphi^{(m)} h^{(m)}} \tag{25}$$

After all the treatment data are calculated, the results are displayed in the form of graphs.

If diverter fluids were injected during the job, it is possible to estimate its efficiency. For that, the following procedure is invented. First, we select the time span with diverter fluid injection. During this time span, we artificially replace the injected diverter fluid with a non-reactive fluid (e.g., water). By that, we zero the skin multiplier within this time span if the skin factor should not change. Second, we take the obtained modified profile of the skin multiplier as an input, and pretending that the bottomhole pressure is unknown, we solve the forward problem using Eqs. (9), (10) and (24). Hence, the results of such forward modeling will represent the wellbore pressure and zonal flow rates without use of diverter fluids. Comparing the solutions of the inverse and forward problems, we estimate the effect brought by the diverter fluid injection.

The key element of the described algorithm is the choice of the appropriate numerical solver for the inverse problem. We test several well-known numerical methods for finding a solution of nonlinear equations (Eq. (9), (10), and (24)). The numerical solver is found to be stable with fast runtime and high accuracy. The details of this study are presented below in Section 3.3. Similarly, a forward problem can be solved almost instantly, and the results obtained in these models are consistent with each other. Below, we verify sensitivity of the solver to several important factors that may change in the treatments, for example, input data provided by engineers (reservoir properties and bottomhole measurements) and time step of integration, typically defined by measurement time sequence.

3.1. Sensitivity to initial conditions

First, we investigate sensitivity of the solution to prescribed initial reservoir conditions. For this study, we consider a two-zone case with synthetic data. We vary initial parameters of the reservoir and estimate its effect on the final skin and zonal fluid distributions. Initially, as a base case, both zones have identical permeability, porosity and lithology that consists of 50% limestone and 50% dolomite. Then, in the second zone, one of reservoir properties has been first incremented to the higher value (case 1), and then decremented to the lower value (case 2). In the first zone, the reservoir properties remain constant and equal to base case values. While changing lithological properties, we assume the second zone

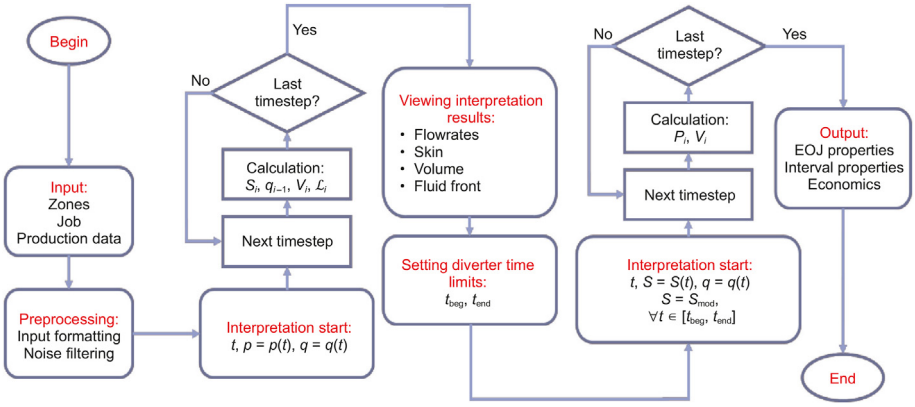

Fig. 2. Scheme of numerical algorithm.

to consist of pure dolomite in case 1 and of pure limestone in case 2, while the first zone is unchanged. We have also similarly changed the viscosity of injected fluid, which penetrate both zones. The values of fluid viscosity and reservoir properties chosen in the study are given in Table 2. The results of the sensitivity study are presented in Fig. 3.

Changes in rock permeability and porosity affect both fluid filtration rates and skin in both zones. These changes reduced difference in the flow rates after the diverter injection (Fig. 3(a)–(d)). On the contrary, the lithology of zones amplifies the difference in zone flow rates and skin during the diversion and post-diversion periods (Fig. 3(e) and (f)). The injected fluid viscosity does not show any significant effect on the filtration rate into each zone, but heavily changes the skin factor (Fig. 3(g) and (h)).

3.2. Sensitivity to time step

As stated before, our model uses recorded data of pressure and injection rate as part of necessary input data. These profiles are measured in fields with prescribed time step. High number of measured points can result in strongly noisy data, while low number of measured points always results in poor resolution of the solution. In general, the inversion algorithm is sensitive to the size of time step and the result can vary significantly. To understand whether our algorithm stability and results depend on it, we calculate the multi-zone case for different number of timesteps. The general information about the observed case is presented in Fig. 4.

The rock consists of pure limestone with variable permeability in all zones. Porosity and compressibility in all zones are the same. Pressure spike from 34-th to 37-th minute represent the injected diverter. Dots show data points which are selected to solve the problem and generally they specify the value of timestep. For a more precise study, we use several sets of these points differing in number. We vary the number of points from 25 to 300, since for most matrix treatment jobs the values from this interval are enough to get an accurate result that will not be affected by either noise or lack of data. Corresponding results are presented in Fig. 5. For a more convenient perception of the effect, only three profiles are presented in the left plot.

Sensitivity of the result to change in the number of time steps is minimal. The mean error is calculated relative to the case with 300 data points. The difference between profiles increases as the number of time steps decreases, but the mean error does not surpass 4%. Prior to the diversion period, the discrepancy is less than 1% and it increases only after injection of a diverter. Starting from minute 40, the difference between 50 and 300 data points is about 7% while between 150 and 300 data points it is less than 2%. In general, the result does not heavily depend on the number of timesteps, and all profiles are similar.

It is important to show that our algorithm does not heavily depend on the number of timesteps. There are, however, few other parameters that affect stability of the algorithm. Beside the size of time step, the initial number of zones can be a reason for possible errors. In our case, the number of zones increases dimensionality of the problem, which results in more unknown parameters. Eq. (9) reduces to finding a single parameter (skin multiplier) in the first place and calculating the remaining necessary quantities in the second place. Therefore, for any number of zones the given problem always has only one correct solution. The number of zones affects the calculation time, which is studied in Section 3.4.

3.3. Algorithms of nonlinear equation root search

Choosing a numerical method is an essential element in tackling the inverse problem. Different methods can be employed to determine the roots of a nonlinear equation, though not all of them are suitable for all scenarios. We compare three established approaches: the Newton-Raphson method, the Muller method, and the Brent method. One of the simplest and successful solutions for locating roots of a non-linear equation is the secant method. It uses a succession of secant lines to estimate the root of a desired equation. The Newton-Raphson method is a generalization of the secant method, that uses function derivatives instead of secant

Table 2
Parameters for the sensitivity study.

Parameter	Base value	Incremented value	Decremented value	Units
Permeability	10	20	5	mD
Porosity	0.1	0.2	0.05	
Viscosity	1	10	0.1	cp
Dolomite content	50	100	0	%
Limestone content	50	100	0	%

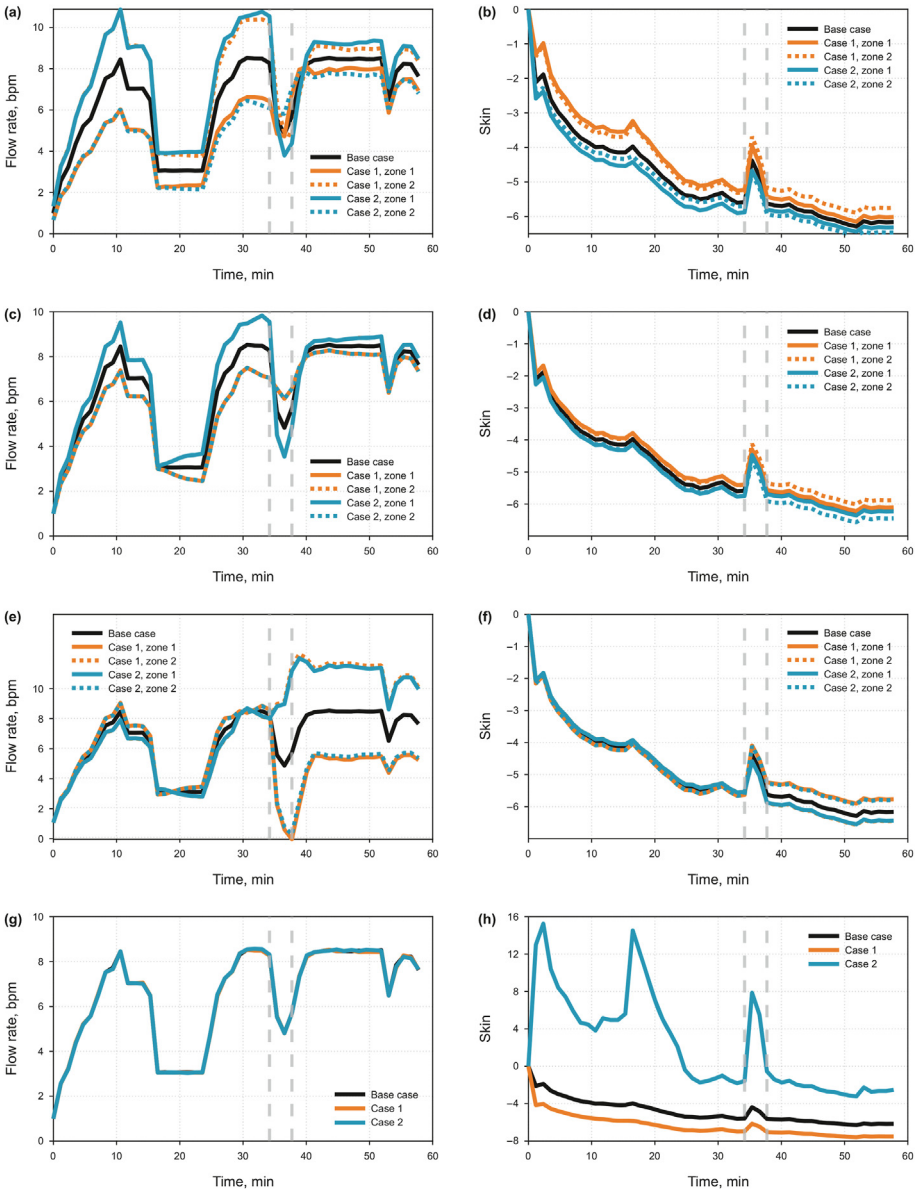

Fig. 3. Sensitivity analysis of calculation results to changes in permeability **(a, b)**, porosity **(c, d)**, lithology **(e, f)** and viscosity **(g, h)**. The target parameter is increased in case 1 and decreased in case 2 for zone 2 only. In zone 1, the target parameter does not change. Dashed gray borders represent the beginning (left line) and end (right line) of diverter injection.

lines. This approach builds a series of tangent lines converging to the function root. The Muller method is known as a quasi-Newton method, where parabolas are built instead of tangent lines. It is slower compared to the Newton-Raphson method; however it has the advantage of being able to search for complex roots. The Brent technique is a combination of secant and bisection approaches.

These three methods are used to solve coupled Eqs. (9), (10) and (24) for the skin multiplier. All other variables are either known from the previous timestep or can be expressed via the skin multiplier. This allows us to convert this system of equations to one equation: $F_n(\widehat{S}_n) = 0$. The function F_n depends on history of the process and, thus, time. In Fig. 6, we illustrate the dependency of function F_n on the skin multiplier at the first timestep (Fig. 6(a)) and later timesteps (Fig. 6(b)).

At the first iteration due to big influence of transient effects, the absolute value of skin multiplier is far from zero. On further iterations, the skin multiplier value is usually close to zero. If the diverter fluid is injected at some time, the skin multiplier again becomes rather high due to the flow redistribution between zones. Even though in the right plot of Fig. 6, the function begins to grow starting from some skin multiplier value, it will never turn to zero second time, which guarantees the uniqueness of the problem's solution. We can conclude that the investigated function $F_n(\widehat{S}_n)$ has only one zero and has no discontinuities. Also, it is possible to use the bracketing which is necessary for several numerical methods.

We use the same field case from Section 3.2, shown in Fig. 4, to investigate application of numerical root-searching methods to our problem. In this study, however, we use both single zone and multi-zonal cases to see whether the complexity of initial equation system restricts the appliance of numerical methods. The single-zone case consists of one zone with the following height and permeability:

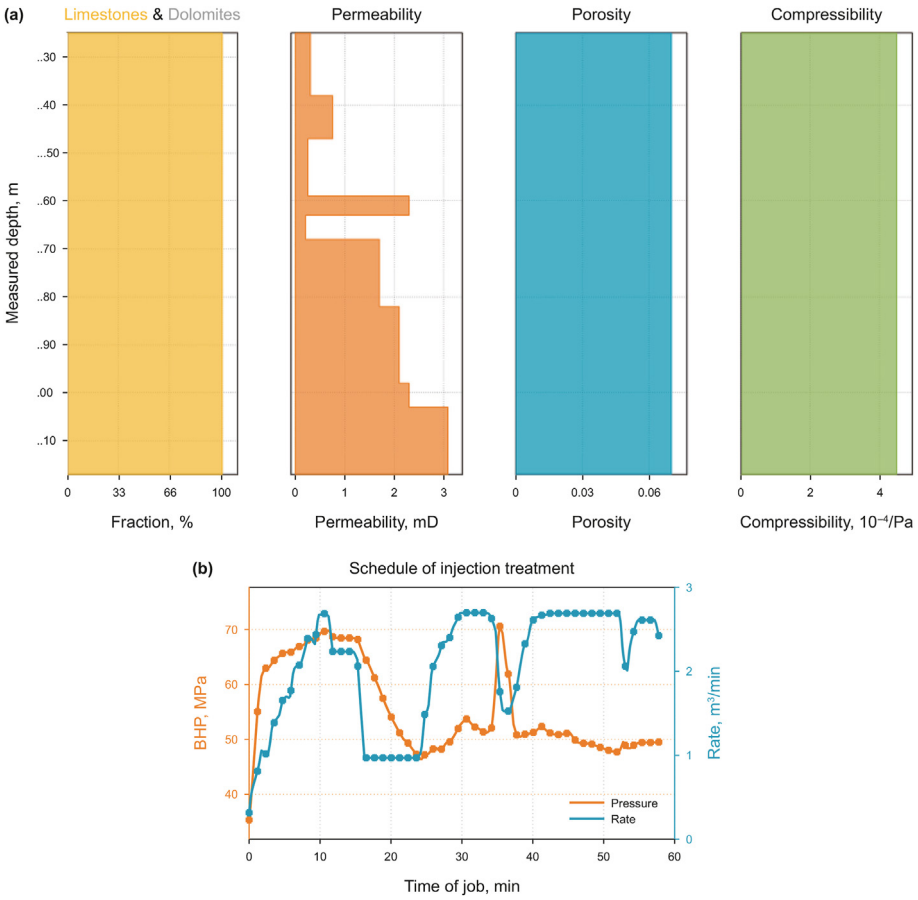

Fig. 4. General description of the studied multizonal case: **(a)** connection of permeability, porosity, and compressibility with measured depth; **(b)** schedule of injection treatment, that consists of pressure (orange) and rate (blue) lines. Dots show points used for calculation which are selected to eliminate noise from data.

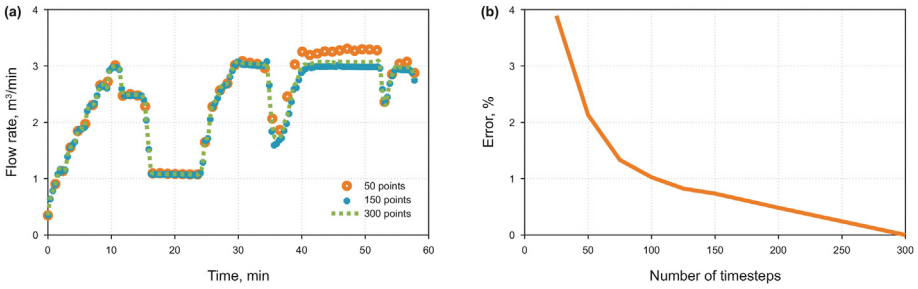

Fig. 5. Sensitivity analysis of the calculation results to number of timesteps in matrix treatment job for multi-zone case: **(a)** flow rate in arbitrary zone; **(b)** mean error of flow rate for different number of timesteps.

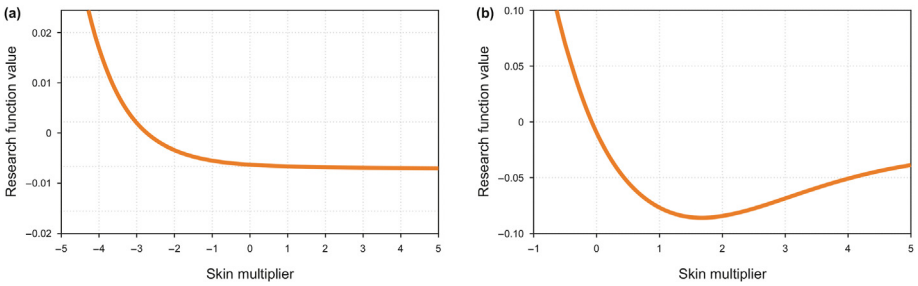

Fig. 6. Behaviour of the studied function depending on the skin multiplier: **(a)** function values for the first iteration, **(b)** the typical function behavior for any other iteration.

$$\begin{cases} k^{(1z)} = \dfrac{\sum\limits_{m=1}^{N} k^{(m)} h^{(m)}}{\sum\limits_{m=1}^{N} h^{(m)}} \\ h^{(1z)} = \sum\limits_{m=1}^{N} h^{(m)} \end{cases} \tag{26}$$

where $k^{(1z)}$ and $h^{(1z)}$ are the permeability and height of the resulting zone; $k^{(m)}$ and $h^{(m)}$ are the permeability and height of corresponding zones in a multi-zonal case. We test three numerical methods: Newton-Raphson, Muller, and Brent methods, using both single-zone and multi-zone cases, except for the Muller method, which is not applied to the multi-zone case. The major drawback of the Muller method is that it generates complex values during the root-searching process even for real values of a skin multiplier. Fig. 7 shows the resulting skin factor calculated from the skin multiplier. For multiple zones (Fig. 7(b)) we plot the results for the zone with the largest absolute skin (i.e., high permeable zone).

All methods for both single-zone and multi-zonal case provide the same results. The difference in the obtained skin factor does not surpass 0.5%. The diverter injection period is between 34 and 37 min. It is characterized by sharp peak of skin factor value and all three methods describe this period in the same way. The convergence of the Newton-Raphson method is a bit faster than that of the Brent's method. Also, the Newton-Raphson method does not require bracketing of the root, which makes it more attractive. In the future studies, we will use this method for all calculations.

3.4. Computational speed

Inverse problem solution may not only be difficult, but also take a long time. The search of the equation root may take several hundred iterations at each time step, so with many timesteps the algorithm can take a long time to find accurate solution. In addition, the zone structure can be complex, so that the number of unknowns and equations greatly increases.

Considering possible delays with convergence, it was decided to implement the algorithm in C++ to use maximum CPU performance and speed up calculations. Four multizonal cases were taken here to investigate the dependency of the number of time intervals on the total computational time of the inverse problem solution. The maximum number of time intervals was set to 500, since the job usually lasts no more than a few hours. The time consumed by the numerical solver exceeds 5 s only for the fourth case if the number of time intervals was 500. Taking in account the results obtained in Section 3.2, we find that the optimal number of timesteps ranges from 50 to 100 points. This optimum is found with the criterion of the error not exceeding 2% and computational time not exceeding 1 s. The results provided in Fig. 8.

4. Verification

4.1. Reciprocity of forward and inverse models

There are several ways to verify correctness of the inverse problem solution. The first and simplest method is to use inverse problem solution as input to the forward problem. If, after solving the latter, a profile of the source data is obtained, then it confirms that the solution of the inverse problem does not contain inaccuracies. The verification is carried out using the following algorithm:

1. Take initial input data, which include the profile of a bottomhole pressure
2. Solve the inverse problem and get time-dependent solution for skin multiplier, skin factor, and flow rate distributions
3. Use the inverse problem solution as an input for the forward problem, and solve it for the bottomhole pressure
4. Compare the original and final pressure profiles

The results of reciprocity of forward and inverse models are presented in Fig. 9 for the single and multiple zones cases. The error in pressure profile reproduction is less than 0.05% for both cases, which means excellent reproducibility of the solution.

4.2. Comparison with exact solution of forward problem

Another way to check correctness of a numerical solution is to

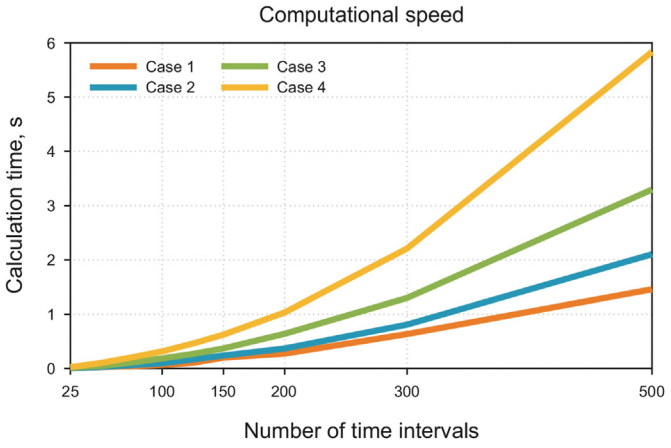

Fig. 8. Calculation time for 4 different cases. Case 1 consists of 8 zones, case 2 consists of 9 zones, case 3 consists of 13 zones, case 4 consists of 58 zones.

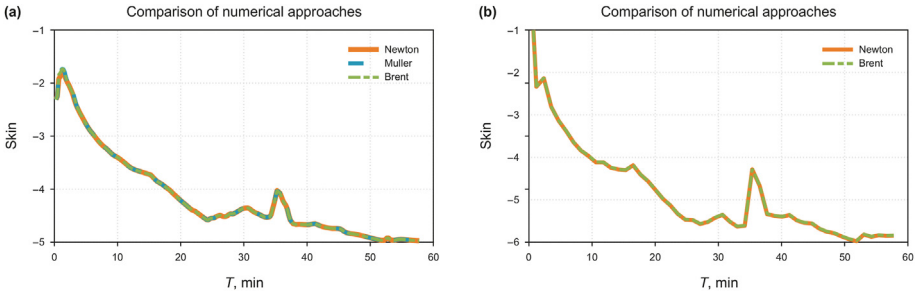

Fig. 7. Comparison of numerical methods for the single-zone case **(a)** and multi-zone case **(b)** in terms of skin factor dependency over time. The resulting skin factor profile in the multi-zone case is taken for the zone with the largest absolute skin factor.

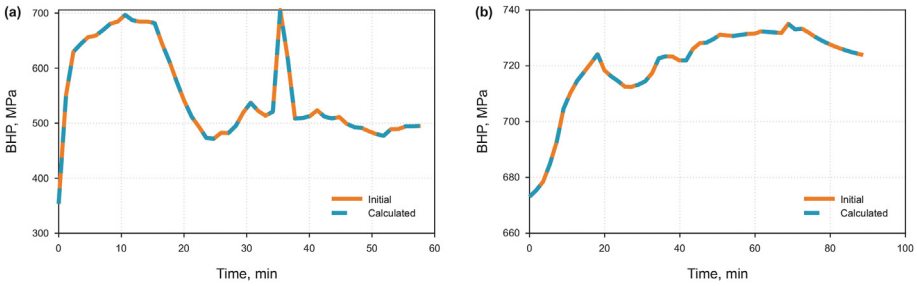

Fig. 9. Reciprocity of inverse and forward solution. Initial bottomhole pressure (orange line) compared with calculated pressure after inverse and forward modelling (blue line) for single-zone **(a)** and multi-zone **(b)** cases.

compare it with the exact analytical solution of the problem. We obtain the analytical solution for a single zone problem, described in Appendix B. For verification, we use the same single-zone case as in section 3.2 and recorded rate data from Fig. 4, bottom. In this case, comparison is possible only for solution of forward problem. To obtain this solution from equation system (Eq. (9)), it is necessary to use prescribed skin factor profile. Here we use four different skin factor profiles, two of which are simple constant skin factors, while two others are more complex (stepwise and harmonical change). The bottomhole pressure calculated for four different skin factor profiles are presented in Fig. 10.

For all skin factor values two calculated pressure profiles are very similar. If there is no skin, both algorithm and analytical solution provide the same result (Fig. 10(a)). For small constant skin factor, the results are similar with sufficiently small discrepancy (Fig. 10(b)). If the skin factor profile is more complex, like stepwise (Fig. 10(c)) or harmonical (Fig. 10(d)) the discrepancy is larger nearby fast pressure variations (peaks or dips), but profiles still look qualitatively similar.

4.3. Comparison with an industrial simulator

4.3.1. Reference solution

Quantitative modeling of the matrix acidizing in carbonates has been following the advancements in theories describing of carbonate rock and acid interaction. By late 1980s, the sandstone acidizing theories were more abundant and better studied in detail than carbonate acidizing, this fact is explained by the surface reaction rate limited nature of sandstone acidizing treatments resulting in easier-to-model, relatively stable displacement front (Daccord et al., 1989). Later, with more attention given to carbonate acidizing research, several theories for quantitative analysis of acid rock interaction research were developed, these theories were well summarized by Fredd and Miller (2000) and Akanni et al. (2017). Progress in quantitative interpretation of the acidizing process resulted in introduction of advanced solutions into the industry. The reference solution (RS) that we use in our work is using algorithms combining wormholing models, laboratory experiments, and concepts described by Fredd and Fogler (1996, 1998), Panga et al. (2002, 2004), Tardy et al. (2007), Ziauddin and Bize (2007). The industry application of these algorithms (at different stages of their evolution) is well documented in the literature (Abdrazakov et al., 2019; Bartko et al., 1997; Kalabayev and Kruglov, 2020; Manakhayev et al., 2018; Ziauddin et al., 2002). As input, the reference solution takes layer-by-layer reservoir properties (permeability, porosity, temperature, reservoir pressure, mineralogy, initial damage composition and depth) and embedded (lab-validated) library of acid-rock interaction parameters for different types of acids. As output, the reference solution produces fluid distribution, wormhole depths, skin factor evolution and other parameters along the treated interval of the wellbore, as long as bottomhole and surface pressures during the injection treatment. The reference solution is using the embedded library of acid-rock interaction parameters, but also accepts manual correction of

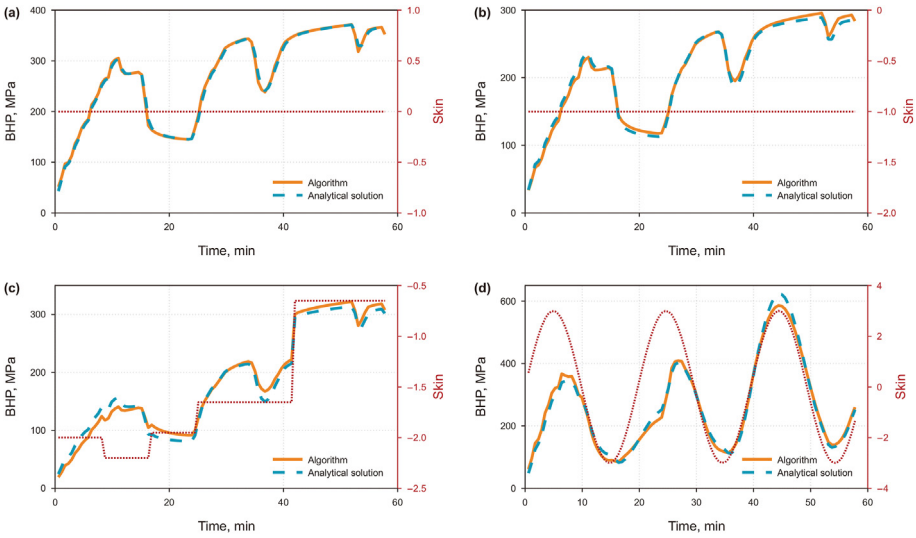

Fig. 10. Comparison of algorithm solution with analytical solution. Orange line is the bottomhole pressure obtained after solving the equation system (Eq. (9)). Blue dashed line is the analytical solution given in Appendix B. Red dotted line is the prescribed skin factor profile which is constant **(a, b)**, stepwise **(c)**, and harmonical **(d)**.

these parameters if the laboratory data differ from the library data. The reference solution is equipped with algorithms of fluid injection method processing, e.g., bullheading into the wellbores, or acid placement with coiled tubing reciprocation. Combination of all these factors allowed for using the described solution as a reference for our study.

The comparison with the reference solution is performed using the following workflow. First, the injection treatment is simulated using reference solution on a given reservoir model with a given pumping schedule. The bottomhole treatment pressure evolution over time produced by the algorithms of the reference solution is taken as a pressure input for our model. Second, the model suggested in this paper is run using the same reservoir model and pumping schedule, but the bottomhole treatment pressure is taken from the output of the reference solution obtained at the previous step. Finally, the fluid distribution is compared between the reference solution and our model. Using this approach, we verify our model, which has simplified acid-rock interaction assumptions, with more rigorous reference solution. In other words, we are testing the statement: "given the same reservoir properties, the same bottomhole pumping schedule (fluid types and rates), and the same bottomhole pressures throughout the treatment, how different our model, in terms of fluid redistribution modelling, from the reference solution used in industry?"

4.3.2. Two zone cases

The main outcome of comparison with a reference solution should be the possibility to calibrate unknown coefficients γ and β in Eq. (23). First, we started with simulation of two-zone cases, to minimize the factor of zone quantity variation, and concentrate on the reservoir properties variation effect. We run 12 two-zone cases, the data are presented in Table 3.

We want to test possible dependencies of coefficients from three different parameters: zonal permeability, lithology content and temperature of acid injected. Each case contains two studies. In the first study, the 15% HCl is pumped for 10 min, after which the inert liquid is injected for 2 min, and lastly, the acid is pumped for another 10 min. The only difference of the second study is that the open path sequence (OPS) diverter is injected instead of the inert liquid. The injection rate was constant (1 bpm) for all cases and studies. To compare our solution with the reference solution, we calculate the volumes that are pumped into each zone immediately after pumping first part of the acid. This is because the first stage is the same in both studies and it is not necessary to take it into account.

Prior to simulations of cases, it is necessary to remove some coefficients from consideration. In the first study there are only 3 unknown coefficients ($\mathscr{T}_0^{\mathrm{L}}$, $\mathscr{T}_0^{\mathrm{D}}$ and γ; $\beta = 1$ for pure acid injection), and in the second one, there are 5 in total (additionally, we have γ and β for diverter). For the first study, we can calculate temperature corrections from empirical dependencies for reaction rates of acid with pure limestone and pure dolomite rocks.

Firstly, we run the first study for all cases. The only reactive fluid injected is acid, so, we suppose $\beta = 1$ since the wormhole growth model is originally written for pure acid. The comparison of cases is presented in Fig. 11. Here and in the future results, Discr is short for discrepancy and means the average difference in injected volumes calculated for all zones.

The correction temperatures $\mathscr{T}_0^{\mathrm{L}}$ and $\mathscr{T}_0^{\mathrm{D}}$ are 80 °C and 151 °C, respectively. The value of parameter γ is 0.0707. This batch of coefficients was achieved after using the MSE method for this study to account for less than 3% discrepancy in all the cases. A small value of the parameter γ implies that there is a dependency on permeability, but in the case of acid injection it is not dominant. It is possible to ignore this dependency completely, but the discrepancy would rise to 5%–7%.

Next, we run the second study for all cases. This is a more complex situation as the inert liquid injection in the middle of the job is changed by the diverter. Now, we cannot suppose that $\beta = 1$ as using initial wormhole growth model for the diverter is incorrect. The comparison of cases is presented in Fig. 12.

The values of parameters γ and β for rock-diverter interactions are 0.5 and 10, respectively. The discrepancy for most of cases is way larger than in the previous study. In case 2, the algorithm overestimates the amount of the fluid redirected while in the cases 8, 9, and 10 the algorithm underestimates it. This can be explained that this model is not initially developed to account for the diverter, so, there is no general set of parameters, that provides a suitable discrepancy for all cases. The cases 5, 6, 7, 11, and 12 show that algorithm has no sensitivity to the diverter, while the reference solution yields a major fluid redirection between the zones. Case 5 has two zones which are the same, so, the diversion can only occur due to gravitational forces, which are ignored in our model. Cases 6 to 12 are calculated under reaction temperature of 120 °C. According to the first study, the distribution of fluids does not depend neither on lithological structure, nor on zone heights. In summary, on the one hand, there is no possibility to find coefficients that would correct describe fluid distribution if the diverter is used during the job. On the other hand, if no diverter is used, the model is correct, and validation is confirmed by the reference solution.

4.3.3. Multiple zones cases

Two zones study provided us a possibility to estimate the unknown coefficients using a wide range of cases with different lithological compositions, permeabilities and heights. However, in most field cases the zone structure is complex, and the reservoir characteristics can vary heavily from zone to zone. To further verify

Table 3
Input for simulated two zone cases. Each field contains data for zone one and zone two divided with slash. Only limestone (Lime) and dolomite (Dolo) are present in the lithological composition of each zone.

Case/Parameter	Zone height, m	Permeability, mD	Lithology content	Temperature, °C (K)
1	10/20	30/30	Limestone/Dolomite	70 (343)
2	10/20	60/6	Dolomite/Dolomite	70 (343)
3	15/15	30/30	Dolomite/Limestone	70 (343)
4	15/15	30/30	Limestone/Dolomite	70 (343)
5	15/15	30/30	Limestone/Limestone	70 (343)
6	15/15	30/30	Limestone/Dolomite	120 (393)
7	10/20	3/3	Limestone/Dolomite	120 (393)
8	10/20	25/15	Limestone/Limestone	120 (393)
9	10/20	30/3	Limestone/Dolomite	120 (393)
10	10/20	30/3	Limestone/Limestone	120 (393)
11	10/20	30/30	Limestone/Dolomite	120 (393)
12	10/20	30/30	70%Lime+30%Dolo/30%Lime+70%Dolo	120 (393)

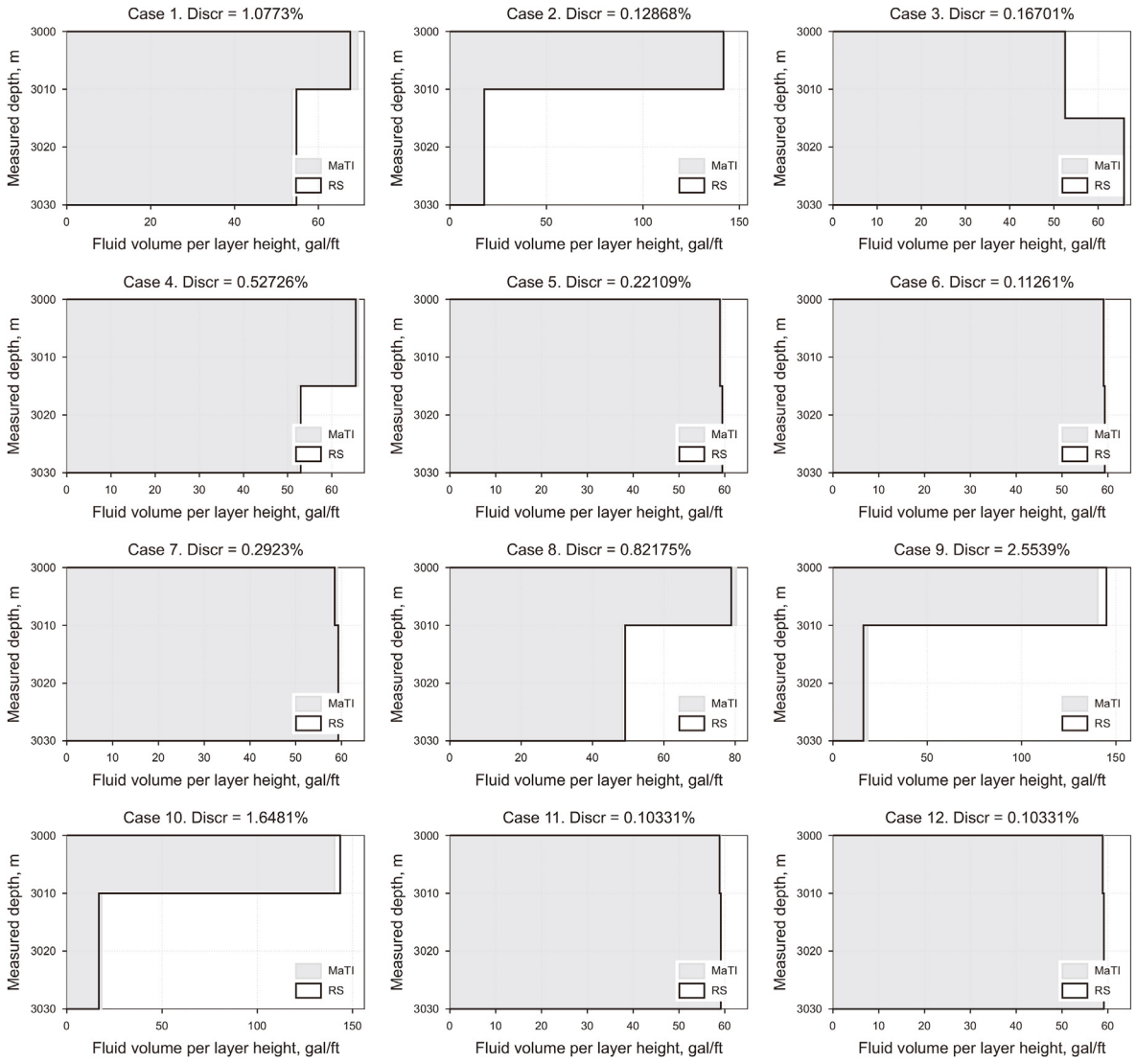

Fig. 11. Comparison of cases in Table 3 within the first study. Gray shading is the result of matrix treatment interpretation algorithm (MaTI); the black contour denotes the reference solution (RS) result.

the correctness of skin defining function, we test it on three multiple zone cases. The brief description of these cases is demonstrated in Fig. 13.

The first case has two zones with large permeability, which take most of injected fluid flow, while the rest of the reservoir is far less permeable. In the other two cases, the permeability distribution is more uniform. Porosity and compressibility profiles are the same in all the cases, as they have less influence on the result and are not studied in detail here. The zones in the second case primarily consist of dolomite, while in the other two cases the dominant material is limestone. Taking parameters obtained in the previous section, we can now run the similar studies. The results are presented in Fig. 14.

When acid is the only reacting fluid, the algorithm has a very good convergence with the reference solution for every multizonal case. The small discrepancy is mainly due to inaccurate calculation of the fluid volume entering the most permeable zone. If the diverter is injected, the resulting discrepancy is much bigger. The algorithm predicts a larger fluid deviation ratio from the most permeable zones to the least permeable. In the first case, two middle zones are mostly depleted in favor of all other zones. In the second and third cases, a large deviation of fluids is observed from upper zones to lower ones. As a result, the algorithm provides a more uniform fluid distribution across all zones than in the reference solution.

5. Interpretation of field cases

The developed interpreter was field tested on the actual acidizing job performed in the Caspian region. The acid treatment was accompanied by the Production Logging (Mukerji, 2013) before and after the job, so the actual value of the model-based interpreter can be clearly seen from this field case.

5.1. Reservoir and well data

The reservoir subjected to acidizing treatment is in the pre-Caspian basin and represented by the limestone formations (Table 4).

The reservoir subjected to acid treatment contains natural fissures and fractures. Speaking about upscaling heterogeneities of fractured carbonate reservoirs to the models with homogeneous

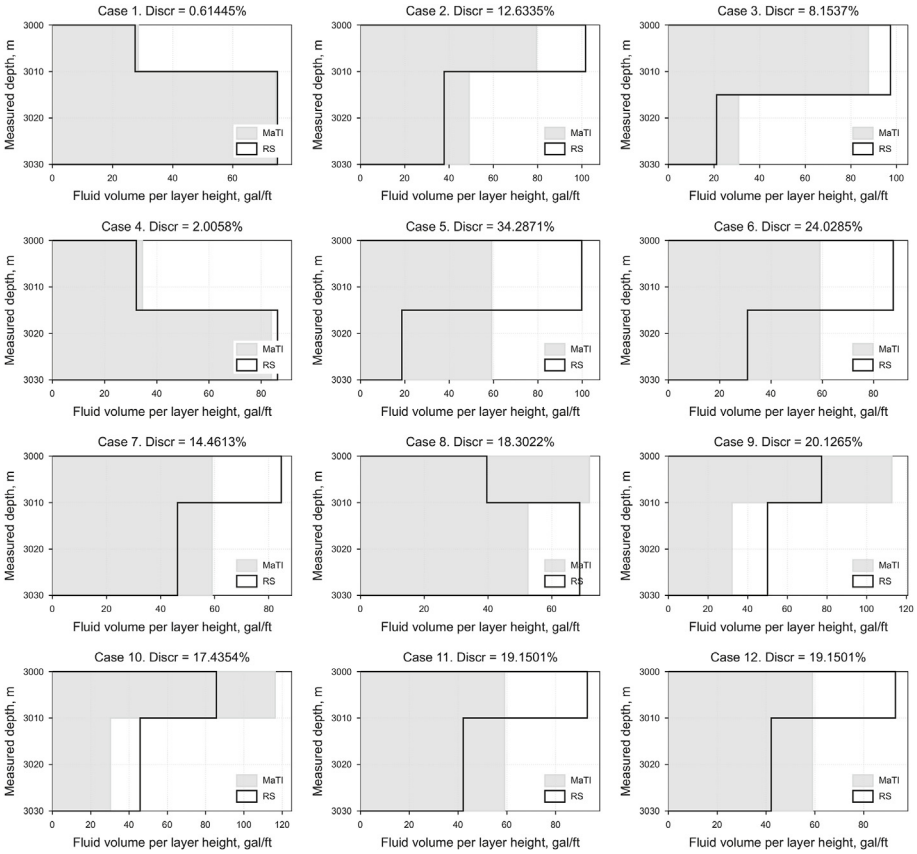

Fig. 12. Comparison of cases in Table 3 within the second study. Gray shading is the result of matrix treatment interpretation algorithm (MaTI); the black contour denotes the reference solution (RS) result.

layers, such method may be reliable if the actual injected fluid penetration distance inside conductive features (fractures, fissures, vugs) is compared to that in high-permeability rock matrix (with respect to which upscaling is done). However, in highly conductive natural fractures mostly free of mineral filling, the fluid can travel dozens of meters along them. Any attempts to upscale and analyze such flow as Darcy's flow in the matrix with so high permeability may lead to significant errors. For the case considered here, natural fractures are thin, as confirmed by Formation Micro Imagers (Wang et al., 2016), have finite conductivity, and filled by secondary precipitated minerals. Given this fact, after upscaling, this reservoir can be well approximated by the Darcy's law.

Considering the above, we created the reservoir's discrete layered model for interpretation. The permeability, lithology, and reservoir pressure distribution for the created model are shown in Fig. 15(a). Before the acidizing job, the fluid production distribution was studied by means of production logging tool (PLT), which estimated actual dynamic production behavior along the wellbore. The PLT showed that majority of production comes from 4 m in the upper wellbore interval, while the middle interval, containing significant hydrocarbon reserves, produces only 25% of hydrocarbons (Fig. 15(b)). Stimulation of the middle zone is then one of key goals of the planned acidizing treatment.

5.2. Acidizing treatment data

As shown above, the wellbore coverage in attempt to deliver acid to the middle zone, was one of the key goals of the treatment. Thus, the pumping schedule for the acidizing treatment consisted of two diverting techniques. First, the inert degradable particles were used in the beginning of the treatment, to plug the most permeable naturally fractured zones. Second, three repeating sequences of main acid and high viscosity diverting acid were employed afterwards. The hydrochloric acid-based single-phase retarded acid (SPRA) was used as a main acid. The viscoelastic surfactant-based (VES) fluid was used as a diverting acid because this fluid increases its own viscosity upon reaction with carbonate. The pumped fluid schedule is shown in Table 5.

For the given actual treatment plot, one can distinguish the obvious trends of pressure gain during diversion stages and pressure drop during active dissolution of the rock by main acids.

In Fig. 16, certain fluctuations are seen at the treatment curves (e.g., at 0:46:00). It is typical for actual injection treatments, and is explained by the following:

- For injection rates, usually several high-pressure pumping units are used. Switching on and off these pumping units for rate control purposes, as well as changing gears, likely result in short fluctuations.
- For recorded pressures, the data are taken from the pressure gauges. These gauges are installed at certain distance from the injection point; thus, the rate-sensitive friction component exists. In addition, in systems with non-negligible compressibility, the so-called "hammer-effect" exists, when the sudden rate change results in pressure oscillations visible as repeating attenuating spikes.

In majority of cases, such fluctuations are not significantly affecting the fluid redistribution picture, so for simplicity and speed of calculations, the suggested interpreter contains the smoothing

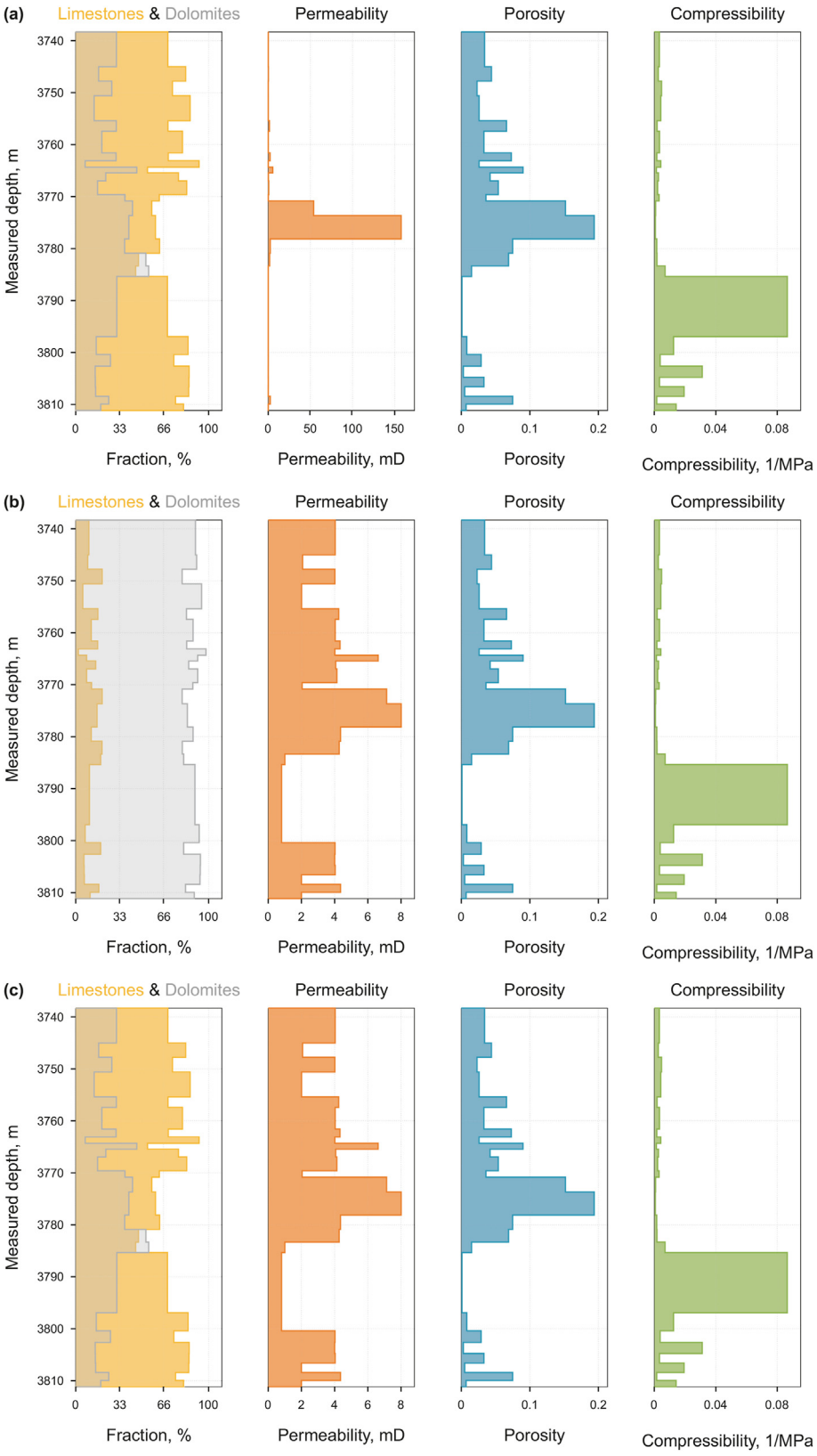

Fig. 13. Structure of multiple zones case. Tracks are reservoir properties (lithology, permeability, porosity, and compressibility, respectively).

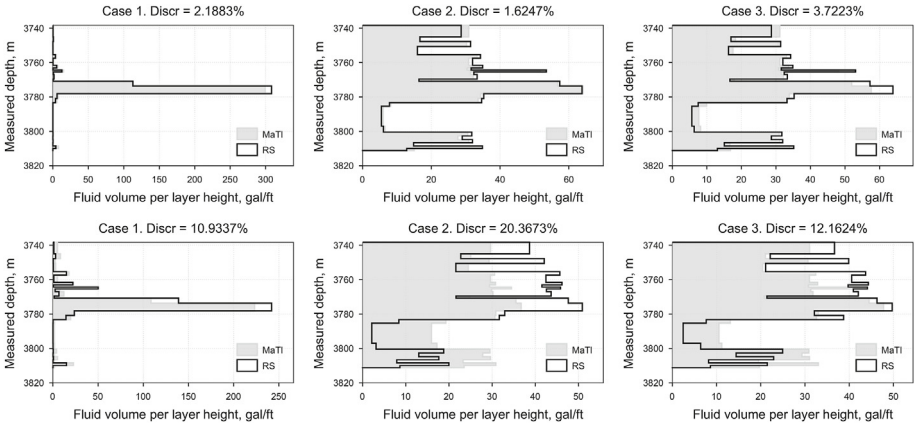

Fig. 14. Comparison of multi zonal cases. First row are rock-acid interactions only; second row are rock-acid and rock-diverter interactions. Gray shading is the result of matrix treatment interpretation algorithm (MaTI); the black contour denotes the reference solution (RS) result.

Table 4
Reservoir and well characteristics of the observed basin.

Parameter	Value	Units
Target reservoir lithology	Limestone (>95%)	
Target reservoir depth	>3500	m
Reservoir temperature	93–105 (366–378)	°C (K)
Target zone permeability	3–20	mD
Reservoir pressure gradient	0.008–0.01	MPa/m
Fluid	Oil, gas condensate	
Well type and geometry	Producer, vertical	
Well completion type	Perforated	
Perforated interval length	~30	m

pre-processing module. After smoothing, the treatment plot for the given well, shown in Fig. 16, results in the filtered line illustrated in Fig. 17.

5.3. Analysis: distribution of diverted volumes

The first step of the analysis is related to selection of the treatment plot intervals where the fluid redistribution analysis is the most beneficial. For the treatment schedule in our example, there are two types of fluid diversion techniques applied: inert degradable particles (step 2 of Table 5) and in-situ gelling acids (steps 4, 5, and 8). These two diversion techniques use different mechanisms of fluid redistribution triggering, in Darcy's law terms: particulates are forming a temporary filter-cake, thus creating additional skin, and in-situ gelling acids act through significant viscosity increase. Generally, the field experience (Abdrazakov et al., 2019) shows that mechanism employed by particulates may result in larger amplitude of pressure increase, compared to viscous-driven methods. On the other hand, the duration of the pressure increase after

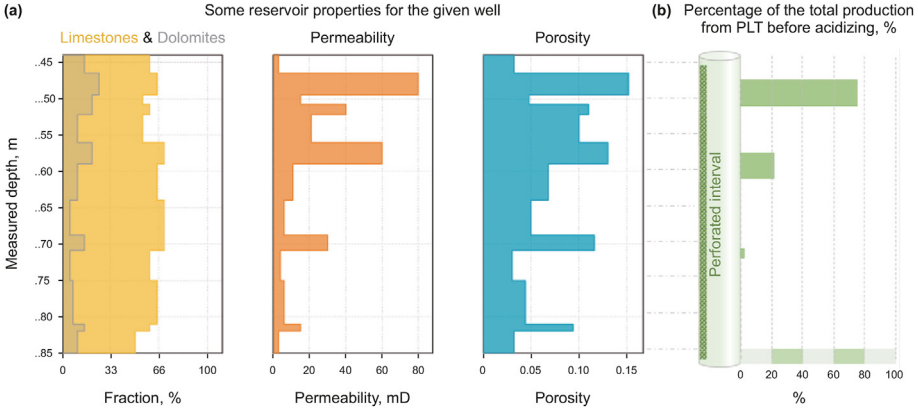

Fig. 15. Three left tracks **(a)** are reservoir properties (lithology, permeability, and porosity, respectively) of the given well in the perforated interval. Rightmost track **(b)** is the pre-acidizing production logging result: the middle zone (depths 50–65 m) is underperforming, thus stimulation of this zone became one of the targets of the acidizing job.

Table 5
The actual measured downhole pumping schedule during acidizing of a given well.

Step	Fluid type	Injected volume, m^3	Pumping rate, m^3/min
1	Initial acid—15% hydrochloric acid	6	1.5
2	Diverter—Inert, neutral, degradable particulates mixture	4	1.5
3–8	VES-based diverter acid alternated with SPRA main acid	90	1.5–4.5
9	15% hydrochloric acid	15	3.5–4
LG	Flush—Water with friction reduction additives	10	3.5

The actual treatment pressure and rate data are shown in Fig. 16. Note that bottomhole pressure shown in this plot is derived from the measured downhole gauge (DHG) data with corrections for the depth difference between DHG and perforations. These corrections consider hydrostatic pressure and calibrated frictions between DHG and perforations.

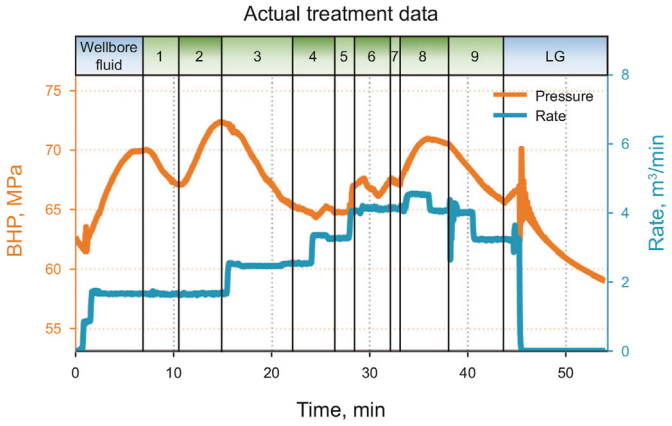

Fig. 16. The actual treatment data. Upper ribbon represents the bottomhole fluid schedule according to Table 5.

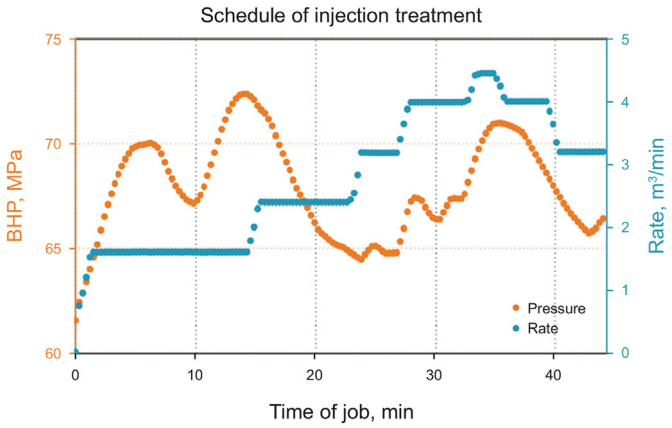

Fig. 17. The actual treatment data filtered after the smoothing procedure. Orange dots are bottomhole pressure versus time. Blue dots are total injection rate versus time.

particulates may be shorter than that after viscous acids if the reactive fluid arrives downhole right after the particles. This can be explained by non-homogeneous localization of the diverting particles' filter cake on the near-wellbore rock face, creating favorable condition for subsequent reactive fluid to bypass the filter-cake. On the contrary, the viscous mass of in-situ gelled acids gains viscosity upon reaction with rock and penetrates deeper into the formation. In this case subsequent portion of lower pH reactive fluids for some period even serves as viscosity-increasing agent supply source.

Another observation from field experience is that the fluid diversion does not necessarily mean the increase of pressure. Instead, it is worth looking at the pressure derivative behavior. Even when pressure decreases during injection (due to the rock or damage dissolution), the slowing down of decline rate can be an indicator of fluid diversion.

Consequently, it was decided to analyze three possible diversion intervals detected on the pumping schedule (Fig. 18). First analysis interval is the step 2 of the treatment schedule, when the particulate diverters caused the pressure increase. Second analysis interval is the step 4, when the in-situ gelled acid's effect slowed down the pressure decline. The third analysis interval is the step 8, when the in-situ gelled acid caused pressure increase, however the simultaneous injection rate increase hinders analysis of the diversion effect.

Analysis of the first selected interval (diverter pumped at step 2) by our interpretation model shows that the significant and obvious

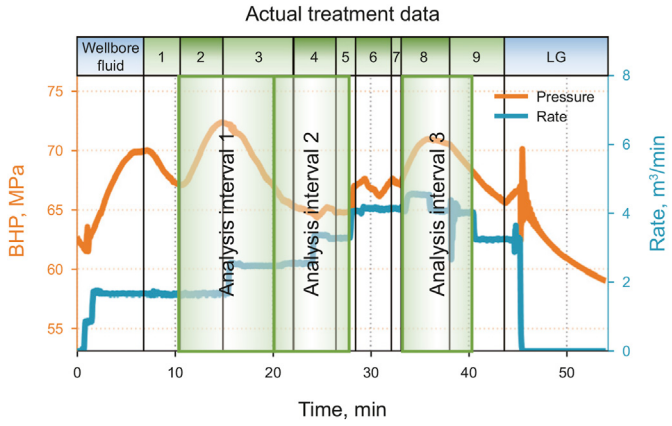

Fig. 18. Three intervals of the injection treatment on the given well, selected for the analysis.

pressure increase caused by a particulate diverter can be attributed to the fluid redistribution from two most permeable intervals into less permeable zones. The diverted fluid volumes can be quantified using our model, as seen from Fig. 19, where approximately 35 gal/ft of fluid is diverted from the second layer (from the top) because of diversion process.

Analysis of the second selected interval (diverter pumped at step 4) shows that after the viscous acid percolation to a formation, the pressure slope change from steep to gentle decline can be attributed to fluid redistribution from the same two most permeable intervals as in the first analysed interval. However, the diverted volumes are 3–4 times less than observed during the diversion in the first interval. That seems quite reasonable, because in the second interval the viscous acid effect was able only to change the decline slope rather than reverse the declining pressure trend to increasing (Fig. 20). In any case, the fluid redistribution is observed from the interpretation model, and thus, our previous empirical statement, that the diversion, to a certain extent, may happen even at pressure decline if the pressure slope changes, found another proof.

The analysis of the third selected interval (diverter pumped at step 8) shows that close to the end of the treatment the character of fluid redistribution between zones changes (Fig. 21(b)). Even though we see relatively similar pressure increase as in the first analysis interval, the affected zones are not the same. Moreover, the previously accepting zones may turn into donating ones: approximately 15 gal/ft of fluid was diverted into the 4th layer (from the top) during the first diversion event (Fig. 19), whereas in the third diversion event, about 20 gal/ft of fluid was diverted from the same layer.

5.4. Validation of MaTI data

After the acidizing treatment and well cleanup, the PLT was run to monitor the fluid redistribution after the treatment. It was noticed that significant redistribution of producing intervals has occurred. Particularly, the middle zone, which was underperforming before the acidizing (25% of total production), became the main producing zone (75%); the upper zone's contribution dropped from 75% to 25%, however the productivity index of the upper zone increased by 20%, i.e., increase of the production from the middle zone has not occurred at the expense of production loss at the upper zone (Fig. 22). Also, PLT showed that after acidizing the bottom interval started to produce.

From the fluid redistribution plots shown in Figs. 19–21, it is

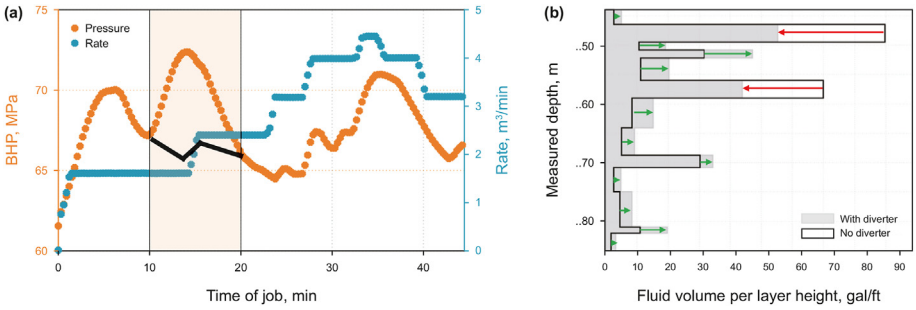

Fig. 19. Analysis of the fluid redistribution at the first analysis interval, during the pressure increase at pumping step 2 (particulate diverter pumped). **(a)** Treatment plot, with highlighted analysis interval (light yellow region); black line inside the interval representing expected approximate pressure behaviour if instead of diverter, fluid of the previous step would have been pumped. **(b)** Output of the interpreter's engine as a well depth (*Y*-axis) vs. fluid volume per zone height (*X*-axis). Gray area on the plot shows fluid distribution from the actual data, i.e., with diversion. Black line contour shows fluid distribution if there was no diversion stage (if pressure would have followed gray dashed line on the left plot). Red arrows highlighted the volumes taken from the given zone because of diversion; green arrows highlight the volumes brought into the zone because of diverter's action.

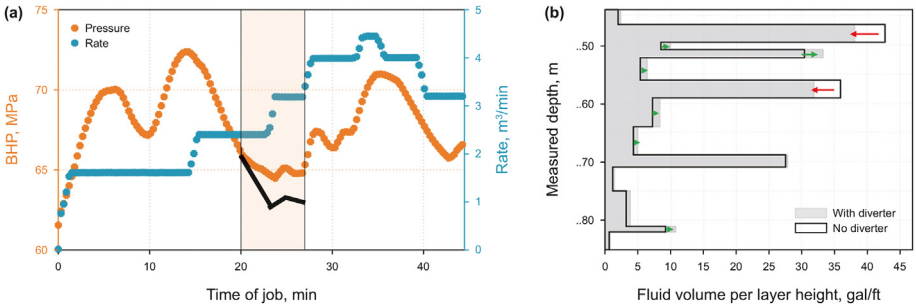

Fig. 20. Analysis of the fluid redistribution at the second analysis interval, during the pressure slope change at pumping step 4, when the viscous diverting acid was pumped. The legend for the plots is the same as in Fig. 19.

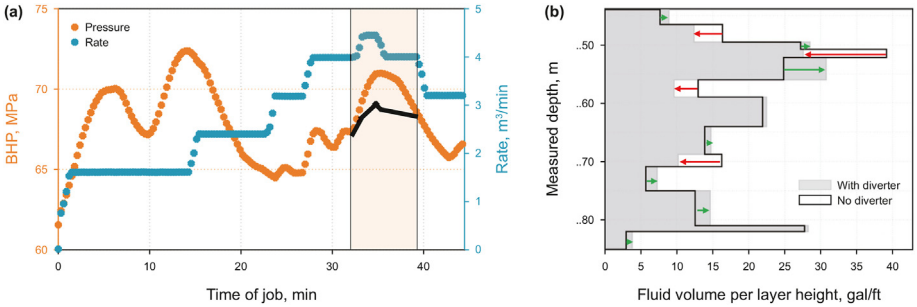

Fig. 21. Analysis of the fluid redistribution at the third analysis interval, during the pressure increase at step 8, when the viscous diverting acid was pumped. The legend for the plots is the same as in Fig. 19.

possible to estimate the cumulative effect of diverters for each zone, calculated by our model, using Eq. (27):

$$\mathrm{CRF}^m = \sum_{i=1}^{n} \mathrm{RF}_i \tag{27}$$

where CRF^m is the cumulative redistributed volume for zone m, during the injection treatment, considering all diversion stages, n is the quantity of the diversion stages, RF_i is the redistributed fluid volume at the individual diversion stage. CRF^m value can be expressed in volume or volume per interval length units.

For the given well, calculation of the CRF for each zone is based on diverted volumes calculated by our model from three analysis intervals and volumes from the diversion step 6 of the pumping schedule, which is not shown as a separate analysis interval.

Comparison of CRF values from our model with the post-treatment PLT shows that the zones which received significant diverted fluid volumes as per our model, showed production increase as per PLT. At the same time, the zones which lost diverted volumes as per our model, in fact experienced production contribution decrease as per PLT. Production redistribution is a function of different parameters, and the effect of a diverter is only one of them. However, in the given example, the diversion pressure signatures are obvious, so the diverter effect should have a significant impact of the fluid redistribution. The calculations by our model provide an approximate quantitative information on this matter, and match with the post-stimulation PLT observations.

Another practical use of the suggested model is optimization of the number of pumping diverter stages. Plots in Fig. 22 (b) and (c) indicate that during the second half of the treatment, the significant flow rate distribution occurs due to the total injection rate increase and action of diverters. If such active flow rate redistribution is

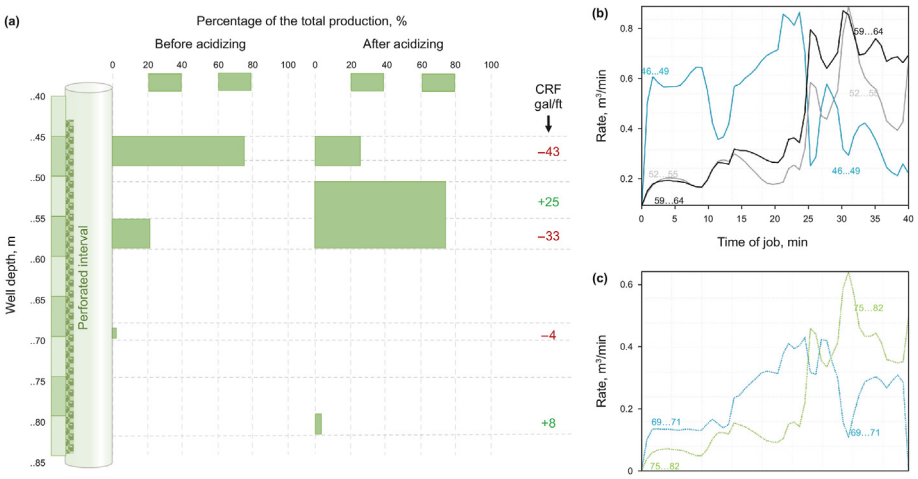

Fig. 22. Validation of the suggested model by the actual post-acidizing PLT. **(a)** The pre-treatment and post-treatment production distributions obtained from PLT, **(b)** and **(c)** fluid rate fluctuations into different zones (depth are shown on the plots) at different time of the treatment.

absent in the pumping job, then it can be an indication that the diversion does not work, and the schedule of diverter fluid pumping should be modified.

6. Discussion

6.1. Extension of suggested model to different types of injection treatments

A common way to optimize and control hydrocarbon recovery processes is to inject special fluids into the rock matrix through wells. The type of injected fluid depends on current challenges and reservoir conditions. Table 6 summarizes various challenges and the injection treatments used to address them.

All injection treatments shown in Table 6 target a certain radius of fluid penetration to achieve the treatment goal. If the target radius is not achieved in the layer of interest, the fluid injection treatment may not reach the goal for which it was designed. In addition, all treatments except acidizing do not require detailed chemical modeling of fluid-rock interaction. Consequently, we believe that the model we propose can be useful for analyzing the fluid redistribution of all the injection treatments shown in Table 6 (the carbonate-acid interaction module can be turned off), except for matrix acidizing in classics, where the chemistry is very complex.

6.2. Extension of suggested model functionality

There are also several possibilities to extend and upgrade the described model. Currently, it accounts only for a single-phase flow, however during matrix treatment jobs multiple fluid phases penetrate the formation. So, effects of relative permeability and phase-to-phase displacement must be considered. It is also important to consider the initial pre-job skin factor in each treated zone, which considers possibly lowered rock permeability. In this model, we have neglected any non-idealities of fluid flow in a well, for example, viscous fluid friction in long horizontal well sections, and gravity effect in vertical wells. We have also ignored fluid friction effect in a limited entry perforation interval, which may become important in horizontal wells.

The presented flow interpretation model is based on the solution of coupled physics and chemistry equations. The model allows to change the law of skin factor buildup in time during acid of diverter injection stages, if that tends to reduce error observed in the model. Artificially changing the duration or excluding some stages of the job allows to vary the design of the whole treatment job and choose the most optimal option for future implementation in the field.

Additionally, it is possible to study fundamentally different models to calculate the matrix treatment problem more accurately. For example, the problem of fracture growth through bedding

Table 6
Challenges associated with hydrocarbon production and injection methods addressing these challenges.

Challenge	Injection treatment to address the challenge	Examples in clastic rocks	Examples in carbonate rocks
Damaged near wellbore zone (high skin factor)	Matrix acidizing	Matrix acidizing using mud acids	Matrix acidizing using hydrochloric acids
Unconsolidated formation particles production	Chemical sand control	Sand consolidating or sand agglomerating fluid injection	
Inorganic scales precipitation	Scale dissolution and Scale inhibition squeezes	Inorganic scale dissolving fluid injection and inorganic scale inhibitor squeezes	
Organic scales forming	Organic scale dissolvers and organic scale inhibitors pumping	Organic scale dissolving fluid injection and organic scale inhibitor squeezes	
Excessive unwanted water production from the productive layers	Chemical water shut-off treatment	Rigid and flowing polymer gels squeezes	Carbonate-compatible rigid and flowing polymer gels squeezes
Excessive gas production from the productive layers	Chemical gas shut-off treatment	Rigid, flowing, and foamed gels squeezes	Carbonate-compatible rigid, flowing, and foamed gels squeezes
Insufficient hydrocarbon recovery factor and poor sweep efficiency around injector wells	Viscous fluid injection to increase recovery factor	Polymer flooding	

interfaces is covered vastly in the industry (Abell et al., 2019; Li and Wu, 2022; Philipp et al., 2013; Tang et al., 2019; Zhang et al., 2007). Many analytical and numerical studies show the influence of hydromechanical properties of rock layers on fracture propagation. They can also benefit acid-rock interaction models, allowing estimations of possible counterflows and acid penetration radius more accurately.

6.3. Use of suggested model for analysis of economic effect of diverters

The study above shows that suggested method provides a quantitative, layer-per-layer analysis of the fluid redistribution during injection. Such analysis has strong practical industrial application (particularly in analysis of the production enhancement) in the following way. First, the volume of fluid added to a given formation layer due to diversion (output of the proposed method) should be converted to the added effective wellbore radius. For example, if acid is being pumped, the added acid volume is converted to the added wormhole length using industry-standard radial mode correlations, then the wormhole length is converted to the added effective borehole radius. Second, the added effective well radius is used to calculate the added production due to the diversion. Finally, the added production is converted into added revenue and compared to the cost of a diverting agent to make further decisions about optimizing the diversion strategy.

6.4. Scientific significance

The current study presents a new approach to solving an inverse problem of transient hydrodynamics in treating formations where measurements of bottomhole pressure and injection rate match each other. The simulations used in most field operations are often hampered by a limited understanding of rock properties. Another obstacle we face is the continuous impact of nonlinear effects that alter the properties of the rock during injection, such as rock damage, creation of hydraulic fractures, natural fracture activation, or chemical reactions with the rock. The forward simulations are affected by both challenges, resulting in discrepancies from reality and physics. This work introduces a distinct method of inverse modeling as an alternative to forward modeling. Through the combination of direct field measurements and the model, this approach provides valuable insights into the changes in rock properties during injection treatments. In this work, instead of calculating the change in rock properties, we choose to determine the skin factor for each treated zone. It revisits the current method of conducting simulations and applies it to a different class of model-based interpretations that we lack in the modeling of acidizing jobs performed in multilayer carbonate formations.

7. Conclusions

In summary, we have developed a new computationally efficient approach to interpreting bottomhole pressure time records during wellbore injection treatments. The developed semi-analytical model describes the fluid flow distribution in complex layered rock and estimates the efficiency of a matrix treatment job in real time or after the job. The model couples both the physical and chemical processes that occur during the injection of chemically active acids and diverter fluids into the rock. It uses direct measurements of pressure and injection rate, so it always has zero mismatch of these with observations, which is often problematic in modern industrial simulators of matrix treatments.

The key innovative results of this work can be formulated as follows:

1. The model correctly solves the inverse problem of fluid filtration, which is proved by comparison with the forward problem solution. Unlike forward models, it solves for the variation of rock skin factor in time, or any other rock property, which is assumed to be known in classical filtration models. Along with the transient change in rock properties during fluid injection, the algorithm predicts fluid distribution among any number of zones with different permeability properties.
2. The proposed method is verified against the industrial reference solution on a realistic geological model consisting of several zones and three different variants of reservoir properties. For all three variants, the discrepancy in redistributed fluid volumes between our approach and the reference solution is within 4% when the diverter is not used, and within 21% when the diverter is used in the pumping schedule.
3. The effectiveness of the proposed approach was evaluated through its application in an acidizing treatment in the Caspian region. The post-treatment PLT has shown a significant increase in production for the zones that received significant diverted fluid volumes, as predicted by our model, and conversely, the decrease in production corresponds to the zones with reduced diverted volumes.
4. The speed and accuracy of the model depend weakly on the complexity of the geological zone profile, the duration of the injection operation and the sampling time.
5. The physicochemical model is sensitive to any number and type of injected acids and diverting agents, which provides an opportunity to control the treatment process and estimate its efficiency.
6. The model can be used to predict future acid treatment jobs in offset wells with the modified injection schedule using the job interpretation performed. It can also be applied to other wellbore injection jobs such as water control, sand control, scale squeeze, and water flooding.
7. The presented model makes an important step forward to development of new type of simulators based on inverse problem solution.

CRediT authorship contribution statement

Igor Reznikov: Writing – review & editing, Writing – original draft, Visualization, Methodology, Investigation, Conceptualization. **Dmitry Abdrazakov:** Writing – review & editing, Writing – original draft, Validation, Methodology. **Dimitry Chuprakov:** Writing – review & editing, Writing – original draft, Supervision, Methodology, Investigation, Conceptualization.

Declaration of competing interest

The authors declare that they have no known competing financial interests or personal relationships that could have appeared to influence the work reported in this paper.

Acknowledgments

Authors express gratitude to Marat Yamborisov for participation at the initial stage of this project, Dr. Valery Shako for valuable remarks about the model, Aleksandra Peshcherenko for assistance with paper preparation, and Schlumberger for permission to publish this work.

Appendix A Improved approximation for transient radial flow

Consider diffusion Eq. (2) with boundary conditions Eqs. (4) and (5). Here we omit the zonal index m. Eq. (2) has no simple exact analytical solution in time domain, so we apply the Laplace transform with respect to time and arrive at the following equation (Matthews and Russell, 1967):

$$\frac{\partial^2 \widehat{p}}{\partial r^2}+\frac{1}{r}\frac{\partial \widehat{p}}{\partial r}-\frac{s}{D}\widehat{p}=0 \tag{A.1}$$

where s is the Laplace parameter. Transformed boundary conditions have the following form:

$$\left.\frac{\partial \widehat{p}}{\partial r}\right|_{r=R_w}=-\frac{q\mu}{2\pi skR_{\mathrm{w}}h} \tag{A.2}$$

$$\widehat{p}|_{r\to\infty}=0 \tag{A.3}$$

Combining Eqs. (A.1)–(A.3) we get the following analytical solution of the problem in the Laplace domain:

$$\widehat{p}(r,s)=\frac{q\mu\sqrt{D/s}}{2\pi khR_{\mathrm{w}}s}\frac{K_0\left(\sqrt{s/D}\,r\right)}{K_1\left(\sqrt{s/D}\,R_{\mathrm{w}}\right)} \tag{A.4}$$

where $K_0(x), K_1(x)$ are the modified Bessel functions of the second kind. Eq. (A.4) has no analytical inversion in time domain, but it is possible to obtain asymptotical approximations of Eq. (A.4) and invert them. The large-time asymptote is well known (Matthews and Russell, 1967):

$$p(r,t)=\frac{q\mu}{4\pi kh}E_1\left(\frac{r^2}{4Dt}\right) \tag{A.5}$$

where $E_1(x)$ is the exponential integral defined as

$$E_1(x)=\int_x^\infty \frac{e^{-u}}{u}du \tag{A.6}$$

The wellbore pressure is then written from Eqs. (A.5)–(A.6) at $r = R_{\mathrm{w}}$.

$$p_{\mathrm{wf}}(T_{\mathrm{D}})=\frac{q\mu}{4\pi kh}E_1\left(\frac{1}{4T_{\mathrm{D}}}\right) \tag{A.7}$$

where we introduced the dimensionless time T_{D}.

$$T_{\mathrm{D}}=\frac{tD}{R_{\mathrm{w}}^2} \tag{A.8}$$

Usually, Eq. (A.7) is the only one used as transient flow solution. It, however, cannot be always applicable to matrix treatment problem. Typical job time is about 1 h, and data can be recorded every second. Eq. (A.7) applied to such short time intervals may result in large errors. For a more accurate result, it is necessary to get early-time asymptotic solution as well. Taking a series expansion of (A.4) at large s ($\sqrt{s/D}R_{\mathrm{w}}\gg 1$) and inverting the result to time domain, we get:

$$p_{\mathrm{wf}}(T_{\mathrm{D}})=\frac{q\mu}{\pi kh}\sqrt{\frac{T_{\mathrm{D}}}{\pi}} \tag{A.9}$$

Accuracy of the obtained solution is determined by the number of terms retained in the series. Eq. (A.9) was obtained using only the first term. Fig. A1 plots both early-time and large-time asymptotic Eqs. (A.7) and (A.9), as well as the accurate inversion of solution Eq. (A.4) as a function of the dimensionless time. The widely used large-time asymptote is valid only for dimensionless time greater than 10, which spans from several seconds to several hours or even days for typical reservoir and fluid injection parameters.

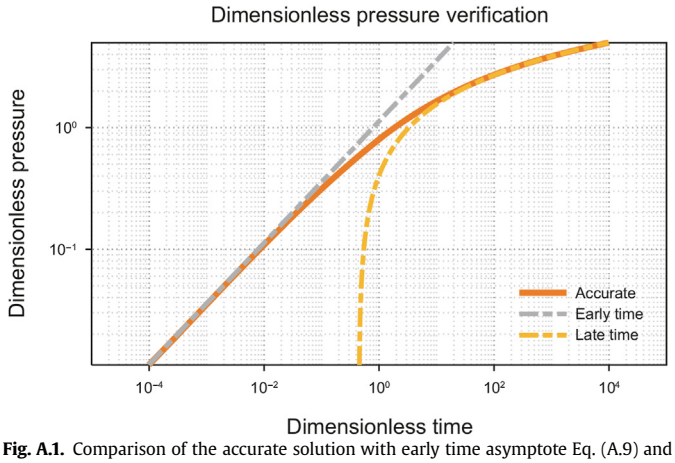

Fig. A.1. Comparison of the accurate solution with early time asymptote Eq. (A.9) and late time asymptote Eq. (A.7). Accurate solution was obtained after the numerical inversion of Eq. (A.4).

Either of those asymptotes is accurate at its own limit, but cannot be applied to the whole time domain (Fig. A1). To develop the universal approximation for the whole time domain, we use the technique proposed by (Clegg, 1967). Using this method, we replace $s = 1/Bt$ and get the following approximation for wellbore pressure:

$$p_{\mathrm{wf}}(T_{\mathrm{D}})=P_{\mathrm{sc}}\sqrt{BT_{\mathrm{D}}}\,\frac{K_0\left(\sqrt{1/BT_{\mathrm{D}}}\right)}{K_1\left(\sqrt{1/BT_{\mathrm{D}}}\right)} \tag{A.10}$$

where $P_{\mathrm{sc}} = q\mu/(2\pi kh)$, B is the inversion coefficient. The inversion coefficient B is found as 1.38, which makes the approximation most accurate.

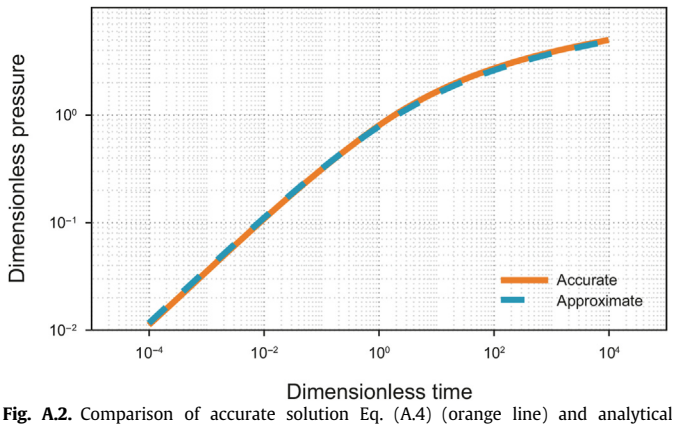

Fig. A.2. Comparison of accurate solution Eq. (A.4) (orange line) and analytical approximation Eq. (A.10) (blue dashed line) with $B = 1.38$.

Fig. A.2 shows convergence of exact and approximate solutions. The mean discrepancy here is less than 3% for $B = 1.38$.

Appendix B Analytical model of reservoir with uniform skin factor distribution

We consider a vertical well placed in a uniform reservoir with constant permeability, porosity, compressibility, fluid viscosity and skin factor. The drainage area is considered radial and infinite in length, so that the transient flow from the well is observed in any arbitrary time given. We decompose the reservoir in two contiguous radial regions: the first interior region, adjacent to the well and having finite radius and constant skin factor, and the second exterior region, having infinite radius and zero skin factor. Both regions are depicted in Fig. B1.

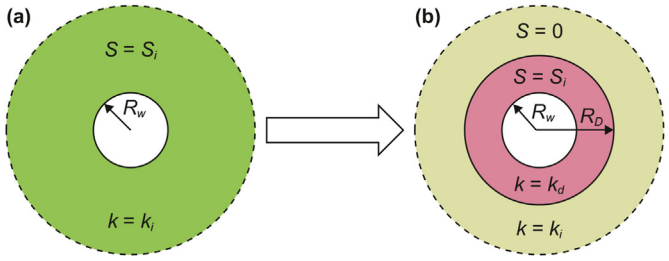

Fig. B.1. Schematic image of unform reservoir **(a)** and two-region configuration **(b)**. The white circle denotes the well with wellbore radius R_w. Light red circle in (b) denotes the stimulated part of the reservoir with increased permeability and finite radius R_D. Green and yellow areas represent the other part of the reservoir.

Given the initial reservoir skin factor S_i, it is possible to relate it with the stimulated zone permeability and radius by means of Hawking formula (Hawkins Jr, 1956):

$$S = \left(\frac{k_i}{k_d} - 1\right)\ln\frac{R_D}{R_w} \tag{B.1}$$

where k_i is the initial reservoir permeability, and k_d is the stimulated region permeability. We now denote the damaged region as region I and the rest of the reservoir as region II. In both regions it becomes possible to solve Eq. (A.1). The general solution along with boundary conditions for region I can be written as

$$\widehat{p}_I = C_1 I_0\left(\sqrt{\frac{s}{DK}}r\right) + C_2 K_0\left(\sqrt{\frac{s}{DK}}r\right) \tag{B.2}$$

$$\left.\frac{\partial\widehat{p}_I}{\partial r}\right|_{r=R_w} = -\frac{q\mu}{2\pi K s k R_w h} \tag{B.3}$$

$$\widehat{p}_I|_{r=R_D} = \widehat{p}_{II}|_{r=R_D} \tag{B.4}$$

where C_1 and C_2 are the unknown coefficients and K is the permeability ratio k_d/k_i. In general case, the permeability ratio is a time-dependent function. For the region II, the similar expressions are obtained:

$$\widehat{p}_{II} = D_1 I_0\left(\sqrt{\frac{s}{D}}r\right) + D_2 K_0\left(\sqrt{\frac{s}{D}}r\right) \tag{B.5}$$

$$\widehat{p}_{II}|_{r\to\infty} = 0 \tag{B.6}$$

$$\widehat{q}_I|_{r=R_D} = \widehat{q}_{II}|_{r=R_D} \tag{B.7}$$

Eqs. (B.4) and (B.7) show that both pressure and flow rates are equal at the interface between the regions. Eqs. (B.2)–(B.7) have in total six unknowns, which makes the system solvable. The coefficients can be written in the following form:

$$C_1 = \frac{q\mu\sqrt{D}}{2\pi k R_w h s^{3/2}\sqrt{K}}\frac{B(s)}{K'_{1,w}A(s) - I'_{1,w}B(s)} \tag{B.8}$$

$$C_2 = \frac{q\mu\sqrt{D}}{2\pi k R_w h s^{3/2}\sqrt{K}}\frac{A(s)}{K'_{1,w}A(s) - I'_{1,w}B(s)} \tag{B.9}$$

$$D_1 = 0 \tag{B.10}$$

$$D_2 = \frac{q\mu\sqrt{D}}{2\pi k R_w h s^{3/2} K}\frac{K'_{1,D}A(s) - I'_{1,D}B(s)}{K'_{1,w}A(s) - I'_{1,w}B(s)}\frac{1}{K_{1,D}} \tag{B.11}$$

$$A(s) = \frac{I'_{1,D}}{I'_{1,w}} + \sqrt{K}\,\frac{I'_{0,D}}{I'_{1,w}}\frac{K_{1,D}}{K_{0,D}} \tag{B.12}$$

$$B(s) = \frac{K'_{1,D}}{I'_{1,w}} - \sqrt{K}\,\frac{K'_{0,D}}{I'_{1,w}}\frac{K_{1,D}}{K_{0,D}} \tag{B.13}$$

where $I_{n,w/D}/K_{n,w/D} = I_n(\sqrt{s/D}R_{w/D})/K_n(\sqrt{s/D}R_{w/D})$, $n = [0, 1]$, $I_{0,1}$ and $K_{0,1}$ are the modified Bessel functions of the first and second kind, respectively. Substituting Eqs. (B.8) and (B.9) in Eq. (B.2) and taking $r = R_w$ gives the relation between bottomhole pressure and damaged zone radius and permeability.

References

Abdrazakov, D., Kalabayev, R., Stepanov, V., Juldugulov, Y., Bekmakhanbet, D., 2019. Integrated approach to diversion during acid treatments in extended intervals, high temperature and fractured reservoirs. In: Paper Presented at the SPE Russian Petroleum Technology Conference, pp. 22–24. https://doi.org/10.2118/196969-MS. Moscow, Russia, October.

Abell, B., Xing, P., Bunger, A., Dontsov, E., Suarez-Rivera, R., 2019. Laboratory investigation of leak-off during hydraulic fracturing into bedding interfaces. SPE/AAPG/SEG Unconv. Resour. Technol. Conf. https://doi.org/10.15530/urtec-2019-900.

Akanni, O.O., Nasr-El-Din, H.A., Gusain, D., 2017. A computational Navier-Stokes fluid-dynamics-simulation study of wormhole propagation in carbonate-matrix acidizing and analysis of factors influencing the dissolution process. SPE J. 22, 2049–2066. https://doi.org/10.2118/187962-PA.

Akanni, O.O.O., Nasr-El-Din, H.A.A., 2015. The accuracy of carbonate matrix-acidizing models in predicting optimum injection and wormhole propagation rates. In: SPE Middle East Oil Gas Show Conf. https://doi.org/10.2118/172575-MS.

Al-Shargabi, M., Davoodi, S., Wood, D.A., Ali, M., Rukavishnikov, V.S., Minaev, K.M., 2023. A critical review of self-diverting acid treatments applied to carbonate oil and gas reservoirs. Petrol. Sci. 20, 922–950. https://doi.org/10.1016/j.petsci.2022.10.005.

Al-Tamimi, Y.K., El-Mzien, N.Y., 1987. Stimulating Multilayered Carbonates in the Upper Zakum Field. Middle East Oil Show. https://doi.org/10.2118/15771-MS.

Ali, M.T., Nasr-El-Din, H.A., 2018. A robust model to simulate dolomite-matrix acidizing. SPE Prod. Oper. 34, 109–129. https://doi.org/10.2118/191136-PA.

Barenblatt, G.I., Entov, V.M., Ryzhik, I.M., 1972. Theory of Nonstationary Filtration of Fluid and Gas. Nedra, Moscow (In Russian).

Bartko, K.M., Acock, A.M., Robert, J.A., Thomas, R.L., 1997. A Field Validated Matrix Acidizing Simulator for Production Enhancement in Sandstone and Carbonates. SPE Eur. Form. https://doi.org/10.2118/38170-MS. Damage Conf.

Biryukov, D., Kuchuk, F.J., 2012. Transient pressure behavior of reservoirs with discrete conductive faults and fractures. Transport Porous Media 95, 239–268. https://doi.org/10.1007/s11242-012-0041-x.

Brent, R.P., 1971. An algorithm with guaranteed convergence for finding a zero of a function. Comput. J. 14, 422–425. https://doi.org/10.1093/comjnl/14.4.422.

Buijse, M., 2000. Understanding wormholing mechanisms can improve acid treatments in carbonate formations. SPE Prod. Facil. 15, 168–175. https://doi.org/10.2118/65068-PA.

Buijse, M., Glasbergen, G., 2005. A semiempirical model to calculate wormhole growth in carbonate acidizing. In: Paper Presented at the SPE Annual Technical Conference and Exhibition, pp. 9–12. https://doi.org/10.2118/96892-MS. Dallas, Texas, October.

Chan, K.S., Flamant, N.C., Helou, H.N., 2003. A Simple, Robust Interpretation Method for Matrix Acidizing Treatments – Part 1: Theoretical Basis and Field Example. Paper Presented at the Middle East Oil Show, Bahrain. https://doi.org/10.2118/

81466-MS. June 2003.
Chandrupatla, T.R., 1997. A new hybrid quadratic/bisection algorithm for finding the zero of a nonlinear function without using derivatives. Adv. Eng. Software 28, 145–149. https://doi.org/10.1016/S0965-9978(96)00051-8.
Cinco-Ley, H., Samaniego, F., 1981. Transient pressure analysis for fractured wells. J. Petrol. Technol. 33, 1749–1766. https://doi.org/10.2118/7490-PA.
Clegg, M.W., 1967. Some approximate solutions of radial flow problems associated with production at constant well pressure. Soc. Petrol. Eng. J. 7, 31–42. https://doi.org/10.2118/1536-PA.
Cohen, C.E., Tardy, P.M.J., Lesko, T., Lecerf, B., Pavlova, S., Voropaev, S., Mchaweh, A., 2010. Understanding diversion with a novel fiber-laden acid system for matrix acidizing of carbonate formations. Proc. - SPE Annu. Tech. Conf. Exhib. 4, 2732–2751. https://doi.org/10.2118/134495-ms.
Crowe, C.W., 1971. Evaluation of diverting oil soluble resin mixtures agents for matrix acidizing as diverting agents for matrix acidizing. In: Paper Presented at the Fall Meeting of the Society of Petroleum Engineers of AIME. New Orleans, Louisiana. https://doi.org/10.2118/3505-MS. October 1971.
Daccord, G., Lenormand, R., 1987. Fractal patterns from chemical dissolution. Nature 325, 41–43. https://doi.org/10.1038/325041a0.
Daccord, G., Lenormand, R., Liétard, O., 1993. Chemical dissolution of a porous medium by a reactive fluid—I. Model for the "wormholing" phenomenon. Chem. Eng. Sci. 48, 169–178. https://doi.org/10.1016/0009-2509(93)80293-Y.
Daccord, G., Touboul, E., Lenormand, R., 1989. Carbonate acidizing: toward a quantitative model of the wormholing phenomenon. SPE Prod. Eng. 4, 63–68. https://doi.org/10.2118/16887-PA.
Doerler, N., Prouvost, L., 1987. Diverting agents: laboratory study and modeling of resultant zone injectivities. In: Paper Presented at the SPE International Symposium on Oilfield Chemistry. https://doi.org/10.2118/16250-MS. San Antonio, Texas, February.
Economides, M.J., Nolte, K.G., 2000. Reservoir Stimulation. Cambridge University Press, Cambridge. https://doi.org/10.1017/CBO9781107415324.004.
Fredd, C.N., Fogler, H.S., 1999. Optimum conditions for wormhole formation in carbonate porous media: influence of transport and reaction. SPE J. 4, 196–205. https://doi.org/10.2118/56995-PA.
Fredd, C.N., Fogler, H.S., 1998. Influence of transport and reaction on wormhole formation in porous media. AIChE J. 44, 1933–1949. https://doi.org/10.1002/aic.690440902.
Fredd, C.N., Fogler, H.S., 1996. Alternative stimulation fluids and their impact on carbonate acidizing. SPE Form. Damage Control Symp. https://doi.org/10.2118/31074-MS.
Fredd, C.N., Miller, M.J., 2000. Validation of carbonate matrix stimulation models. In: SPE Int. Symp. Form. Damage Control. Lafayette, Louisiana. https://doi.org/10.2118/58713-MS.
Fredd, C., 2000. Dynamic model of wormhole formation demonstrates conditions for effective skin. In: SPE Permian Basin Oil and Gas Recovery Conference. https://doi.org/10.2118/59537-MS. Midland, Texas, March 2000.
Furui, K., Burton, R.C., Burkhead, D.W., Abdelmalek, N.A., Hill, A.D., Zhu, D., Nozaki, M., 2011. A comprehensive model of high-rate matrix-acid stimulation for long horizontal wells in carbonate reservoirs: Part I—scaling up core-level acid wormholing to field treatments. SPE J. 17, 271–279. https://doi.org/10.2118/134265-PA.
Gdanski, R., 1999. A fundamentally new model of acid wormholing in carbonates. In: Paper Presented at the SPE European Formation Damage Conference. https://doi.org/10.2118/54719-MS. The Hague, Netherlands.
Hawkins Jr., M.F., 1956. A note on the skin effect. J. Petrol. Technol. 8, 65–66. https://doi.org/10.2118/732-G.
Hill, A.D., Zhu, D., 1996. Real time monitoring of matrix acidizing including the effects of diverting agents. SPE Prod. Facil. 11, 95–101. https://doi.org/10.2118/28548-PA.
Hoefner, M.L., Fogler, H.S., 1988. Pore evolution and channel formation during flow and reaction in porous media. AIChE J. 34, 45–54. https://doi.org/10.1002/aic.690340107.
Huang, T., Hill, A.D., Schechter, R.S., 2000. Reaction rate and fluid loss: the keys to wormhole initiation and propagation in carbonate acidizing. SPE J. 5, 287–292. https://doi.org/10.2118/65400-PA.
Huang, T., Zhu, D., Hill, A.D., 1999. Prediction of wormhole population density in carbonate matrix acidizing. In: SPE European Formation Damage Conference. https://doi.org/10.2118/54723-MS. The Hague, Netherlands.
Jia, C., Sepehrnoori, K., Huang, Z., Yao, J., 2021. Modeling and analysis of carbonate matrix acidizing using a new two-scale continuum model. SPE J. 26, 2570–2599. https://doi.org/10.2118/205012-PA.
Kalabayev, R., Kruglov, R., 2020. Combining technologies optimises acid stimulation: field case studies in Kazakhstan. SPE Asia Pacific Oil Gas Conf. Exhib. https://doi.org/10.2118/202223-MS.
Kuchuk, F., Biryukov, D., Fitzpatrick, T., 2015. Fractured-reservoir modeling and interpretation. SPE J. 20, 983–1004. https://doi.org/10.2118/176030-pa.
Li, J., Wu, K., 2022. An efficient model for hydraulic fracture height growth considering the effect of bedding layers in unconventional shale formations. SPE J. 27, 3740–3756. https://doi.org/10.2118/210572-PA.
Lund, K., Foglers, H.S., Mccune, C.C., Ault, J.W., 1975. Acidization-II. The dissolution of calcite in hydrochloric acid. Chem. Eng. Sci. 30, 825. https://doi.org/10.1016/0009-2509(75)80047-9, 335.
Lund, R., Foglerf, H.S., Mccune, C.C., 1973. Acidization-I. The dissolution of dolomite in hydrochloric acid. Chem. Eng. Sci. 28, 691–700. https://doi.org/10.1016/0009-2509(77)80003-1.
Manakhayev, R., Abilgaziyeva, N., Bopiyev, C., Saduakassov, B., Abdrazakov, D., Stepanov, V., Se, Y., Clarke, J., Kamispaev, A., Tyre, R., Nurmanov, S., Ismailov, B., Argynov, D., 2018. Staged acid stimulation initiative in giant carbonate reservoir. SPE Annu. Casp. Tech. Conf. Exhib. https://doi.org/10.2118/192565-MS.
Matthews, C.S., Russell, D.G., 1967. Pressure Buildup and Flow Tests in Wells. Society of Petroleum Engineers of AIME.
McLeod, H.O., Coulter, A.W., 1969. The stimulation treatment pressure record - an overlooked formation evaluation tool. J. Petrol. Technol. 21, 951–960. https://doi.org/10.2118/2287-PA.
Montgomery, C.T., Jan, Y.-M., Niemeyer, B.L., 1995. Development of a matrix-acidizing stimulation treatment evaluation and recording system. SPE Prod. Facil. 10, 219–224. https://doi.org/10.2118/26579-PA.
Muller, D.E., 1956. A method for solving algebraic equations using an automatic computer. Math. Comput. 10, 208–215. https://doi.org/10.1090/S0025-5718-1956-0083822-0.
Núñez, W., Leal, J., Malik, A., Solares, J.R., Sierra, L., Izquierdo, G., 2009. Multilayered reservoir stimulation: case study of effective acid diversion achieved using the associative polymer treatment diverting agent in Khuff carbonate reservoir wells in Saudi Arabia's Ghawar Field. In: Asia Pacific Oil Gas Conf. Exhib. https://doi.org/10.2118/123442-MS.
Paccaloni, G., 1979. New method proves value of stimulation planning. Oil Gas J. 77, 155–160.
Paccaloni, G., Tambini, M., Galoppini, M., 1988. Key factors for enhanced results of matrix stimulation treatments. In: Paper Presented at the SPE Formation Damage Control Symposium. https://doi.org/10.2118/17154-MS. Bakersfield, California, February.
Panga, M.K.R., Balakotaiah, V., Ziauddin, M., 2002. Modeling, simulation and comparison of models for wormhole formation during matrix stimulation of carbonates. SPE Annu. Conf. Exhib, Tech. https://doi.org/10.2118/77369-MS.
Panga, M.K.R., Ziauddin, M., Gandikota, R., Balakotaiah, V., 2004. A new model for predicting wormhole structure and formation in acid stimulation of carbonates. SPE Int. Symp. Exhib. Form. Damage Control. https://doi.org/10.2118/86517-MS.
Panjalizadeh, H., Safari, A.R., Kamani, M., 2021. An efficient interpretation method for matrix acidizing evaluation and optimization in long heterogeneous carbonate Reservoirs. SPE Prod. Oper. 36, 780–794. https://doi.org/10.2118/203411-PA.
Parn-anurak, S., Engler, T.W., 2005. Modeling of fluid filtration and near-wellbore damage along a horizontal well. J. Pet. Sci. Eng. 46, 149–160. https://doi.org/10.1016/j.petrol.2004.12.003.
Philipp, S., Sar, F., Gudmundsson, A., 2013. Effects of mechanical layering on hydrofracture emplacement and fluid transport in reservoirs. Front. Earth Sci. 1. https://doi.org/10.3389/feart.2013.00004.
Pongratz, R., Kontarev, R., Robertson, B., 2005. Optimizing matrix acid treatments in a multilayered reservoir in Russia by applying different diversion techniques. SPE Eur. Form. Damage Conf. https://doi.org/10.2118/94485-MS.
Prouvost, L.P., Economides, M.J., 1989. Applications of real-time matrix acidizing evaluation method. SPE Prod. Eng. 4, 401–407. https://doi.org/10.2118/17156-pa.
Prouvost, L.P., Economides, M.J., 1987. Real-time evaluation of matrix acidizing treatments. J. Pet. Sci. Eng. 1, 145–154. https://doi.org/10.1016/0920-4105(87)90005-2.
Pye, D., Gallus, J., Kemp, J., 1970. Placement control boosts well-stimulation results. Oil Gas J. 68, 76–80.
Ramondenc, P., Lecerf, B., Tardy, P.M., 2013. Achieving optimum placement of stimulating fluids in multilayered carbonate reservoirs: a novel approach. In: SPE Annu. Tech. Conf. Exhib. https://doi.org/10.2118/166184-MS.
Ridders, C., 1979. A new algorithm for computing a single root of a real continuous function. IEEE Trans. Circ. Syst. 26, 979–980. https://doi.org/10.1109/TCS.1979.1084580.
Schwalbert, M.P., Zhu, D., Hill, A.D., 2017. Extension of an empirical wormhole model for carbonate matrix acidizing through two-scale continuum 3D simulations. In: SPE Eur. Featur. 79th EAGE Conf. Exhib. https://doi.org/10.2118/185788-MS.
Tang, J., Wu, K., Zuo, L., Xiao, L., Sun, S., Ehlig–Economides, C., 2019. Investigation of rupture and slip mechanisms of hydraulic fractures in multiple-layered formations. SPE J. 24, 2292–2307. https://doi.org/10.2118/197054-PA.
Tardy, P.M.J., Lecerf, B., Christanti, Y., 2007. An experimentally validated wormhole model for self-diverting and conventional acids in carbonate rocks under radial flow conditions. SPE - Eur. Form. Damage Conf. Proceedings, EFDC 2, 851–866. https://doi.org/10.2118/107854-ms.
Turegeldieva, K.A., Zhapbasbayev, U.K., Assilbekov, B.K., Zolotukhin, A.B., 2016. Matrix acidizing modeling of near-wellbore with reduced reservoir properties (part 1). Neft. khozyaystvo - Oil Ind. 2016, 50–54 (in Russian).
Wang, Y., Hill, A.D., Schechter, R.S., 1993. The optimum injection rate for matrix acidizing of carbonate formations. In: Paper Presented at the SPE Annual

Technical Conference and Exhibition. https://doi.org/10.2118/26578-MS. Houston, Texas, October.
Yuan, T., Qin, G., 2020. Numerical investigation of wormhole formation during matrix acidizing of carbonate rocks by coupling Stokes-Brinkman equation with reactive transport model under radial flow conditions. In: SPE Int. Conf. Exhib. Form. Damage Control. https://doi.org/10.2118/199262-MS.
Zhang, X., Jeffrey, R.G., Thiercelin, M., 2007. Deflection and propagation of fluid-driven fractures at frictional bedding interfaces: a numerical investigation. J. Struct. Geol. 29, 396–410. https://doi.org/10.1016/j.jsg.2006.09.013.
Ziauddin, M., Bize, E., 2007. The effect of pore-scale heterogeneities on carbonate stimulation treatments. In: SPE Middle East Oil Gas Show Conf. https://doi.org/10.2118/104627-MS.
Ziauddin, M., Kotlar, H.K., Vikane, O., Frenier, W., Poitrenaud, H., 2002. The use of a virtual chemistry laboratory for the design of matrix stimulation treatments in the Heidrun Field. Eur. Pet. Conf. https://doi.org/10.2118/78314-MS.